



Review

# Imaging Techniques in Alzheimer's Disease: A Review of Applications in Early Diagnosis and Longitudinal Monitoring

Wieke M. van Oostveen <sup>1</sup> and Elizabeth C. M. de Lange <sup>2,\*</sup>

<sup>1</sup> Faculty of Science, Leiden University, Einsteinweg 55, 2333 CC Leiden, The Netherlands; w.m.van.oostveen@umail.leidenuniv.nl

<sup>2</sup> Division of Systems Biomedicine and Pharmacology, Leiden Academic Centre of Drug Research, Leiden University, Einsteinweg 55, 2333 CC Leiden, The Netherlands

\* Correspondence: ecmdelange@lacdr.leidenuniv.nl; Tel.: +31-71-527-6330

**Abstract:** Background. Alzheimer's disease (AD) is a progressive neurodegenerative disorder affecting many individuals worldwide with no effective treatment to date. AD is characterized by the formation of senile plaques and neurofibrillary tangles, followed by neurodegeneration, which leads to cognitive decline and eventually death. Introduction. In AD, pathological changes occur many years before disease onset. Since disease-modifying therapies may be the most beneficial in the early stages of AD, biomarkers for the early diagnosis and longitudinal monitoring of disease progression are essential. Multiple imaging techniques with associated biomarkers are used to identify and monitor AD. Aim. In this review, we discuss the contemporary early diagnosis and longitudinal monitoring of AD with imaging techniques regarding their diagnostic utility, benefits and limitations. Additionally, novel techniques, applications and biomarkers for AD research are assessed. Findings. Reduced hippocampal volume is a biomarker for neurodegeneration, but atrophy is not an AD-specific measure. Hypometabolism in temporoparietal regions is seen as a biomarker for AD. However, glucose uptake reflects astrocyte function rather than neuronal function. Amyloid- $\beta$  ( $A\beta$ ) is the earliest hallmark of AD and can be measured with positron emission tomography (PET), but  $A\beta$  accumulation stagnates as disease progresses. Therefore,  $A\beta$  may not be a suitable biomarker for monitoring disease progression. The measurement of tau accumulation with PET radiotracers exhibited promising results in both early diagnosis and longitudinal monitoring, but large-scale validation of these radiotracers is required. The implementation of new processing techniques, applications of other imaging techniques and novel biomarkers can contribute to understanding AD and finding a cure. Conclusions. Several biomarkers are proposed for the early diagnosis and longitudinal monitoring of AD with imaging techniques, but all these biomarkers have their limitations regarding specificity, reliability and sensitivity. Future perspectives. Future research should focus on expanding the employment of imaging techniques and identifying novel biomarkers that reflect AD pathology in the earliest stages.

**Keywords:** Alzheimer's disease; imaging techniques; early diagnosis; longitudinal monitoring; amyloid- $\beta$ ; tau; MRI; PET



**Citation:** van Oostveen, W.M.; de Lange, E.C.M. Imaging Techniques in Alzheimer's Disease: A Review of Applications in Early Diagnosis and Longitudinal Monitoring. *Int. J. Mol. Sci.* **2021**, *22*, 2110. <https://doi.org/10.3390/ijms22042110>

Academic Editor:  
Arkadiusz Orzechowski

Received: 15 December 2020  
Accepted: 16 February 2021  
Published: 20 February 2021

**Publisher's Note:** MDPI stays neutral with regard to jurisdictional claims in published maps and institutional affiliations.



**Copyright:** © 2021 by the authors. Licensee MDPI, Basel, Switzerland. This article is an open access article distributed under the terms and conditions of the Creative Commons Attribution (CC BY) license (<https://creativecommons.org/licenses/by/4.0/>).

## 1. Introduction

Alzheimer's disease (AD) is a progressive neurodegenerative disorder resulting in memory loss, cognitive impairment, behavioural changes and eventually death [1]. AD is the most common cause of dementia and is predicted to affect more than 152 million people in 2050 [2]. The disease is neuropathologically characterized by the deposition of abnormal protein resulting in the formation of extracellular senile plaques and intracellular neurofibrillary tangles (NFTs) [3,4]. The senile plaques contain primarily neurotoxic amyloid- $\beta$  ( $A\beta$ ) [5], whereas NFTs consist of abnormal hyperphosphorylated tau aggregates [6,7]. Although the contribution of abnormal protein deposition to AD is recognized,

the exact pathogenesis of AD is complex [8], and definitive diagnosis can only be assured post-mortem by histology staining of the brain [9]. Currently, AD is the only cause of death in the top ten deaths globally for which no effective therapeutic treatment is available, and there are no registered drugs to slow down disease progression [10]. Therefore, much effort is put into understanding the pathogenesis of AD for the development of therapeutic agents [11].

In AD, neuropathological changes occur up to thirty years before clinical manifestation of the disease [12]. The initial pathological event in AD is A $\beta$  deposition, which contributes to the formation of senile plaques. Likewise, hyperphosphorylation results in NFTs, leading to neuronal loss, brain atrophy, neurotoxicity, and ultimately cognitive decline [7]. In 1991, Braak and Braak characterized the spread of NFTs across the brain and defined six different stages [3]. These Braak stages correspond with the expansion of NFTs from transentorhinal regions (stage I/II) to limbic areas (stage III/IV) and neocortical regions (stage V/VI) as AD progresses.

The above listed events succeed and overlap each other and, therefore, AD is seen as a continuum with pathological changes and clinical symptoms corresponding to the disease stage [13] (Figure 1). Since damage inflicted by these events can surpass a certain neuropathological threshold beyond which any treatment will be unsuccessful, it has been suggested that therapeutic agents should focus on halting neurodegeneration in the silent phase of AD before it becomes too severe [14–16]. Therefore, sensitive and specific methods are needed to diagnose AD in the early or preclinical stage [1]. Nowadays, the field of research focuses on identifying so-called biomarkers, which are physiological, chemical or anatomical parameters called biomarkers that effectively reflect certain pathopsychological processes in AD [17]. These biomarkers can be categorized into three different classes based on the type of pathophysiology the biomarker tracks. In this so-called “A/T/N” system, “A” refers to biomarkers measuring A $\beta$  deposition, “T” indicates biomarkers sensitive for tau and “N” the value of biomarkers perceptive for neurodegeneration [18]. This framework is adaptable and can continuously be expanded if new biomarkers become available [19].

An ideal biomarker is inexpensive, easy to monitor and non-invasive and, therefore, will barely harm a patient. Moreover, a good biomarker has high sensitivity and predictive qualities for the specific pathological event [15]. Eventually, biomarkers could offer a diagnostic tool to detect the disease in early stages, thereby providing the opportunity to delay disease progression or even impede the clinical manifestation of the disease [20]. Additionally, monitoring these biomarkers over time could give insight into disease progression and be utilized to track the effectiveness of disease-modifying therapeutics.

In this review, we focus on biomarkers that can be tracked with structural or functional neuroimaging techniques, such as magnetic resonance imaging (MRI) and positron emission tomography (PET), respectively. The aim of this review is to give an overview of established biomarkers for the early diagnosis and longitudinal monitoring of AD and discuss their feasibility and potential drawbacks. First, we shed light on current biomarkers for the early diagnosis of AD and longitudinal monitoring of disease progression. These biomarkers are reviewed based on their diagnostic utility, benefits and limitations. Subsequently, we introduce new biomarkers and applications of imaging techniques that show promising results for the early diagnosis or longitudinal monitoring of Alzheimer’s disease. Finally, we summarize our findings and provide future perspectives.

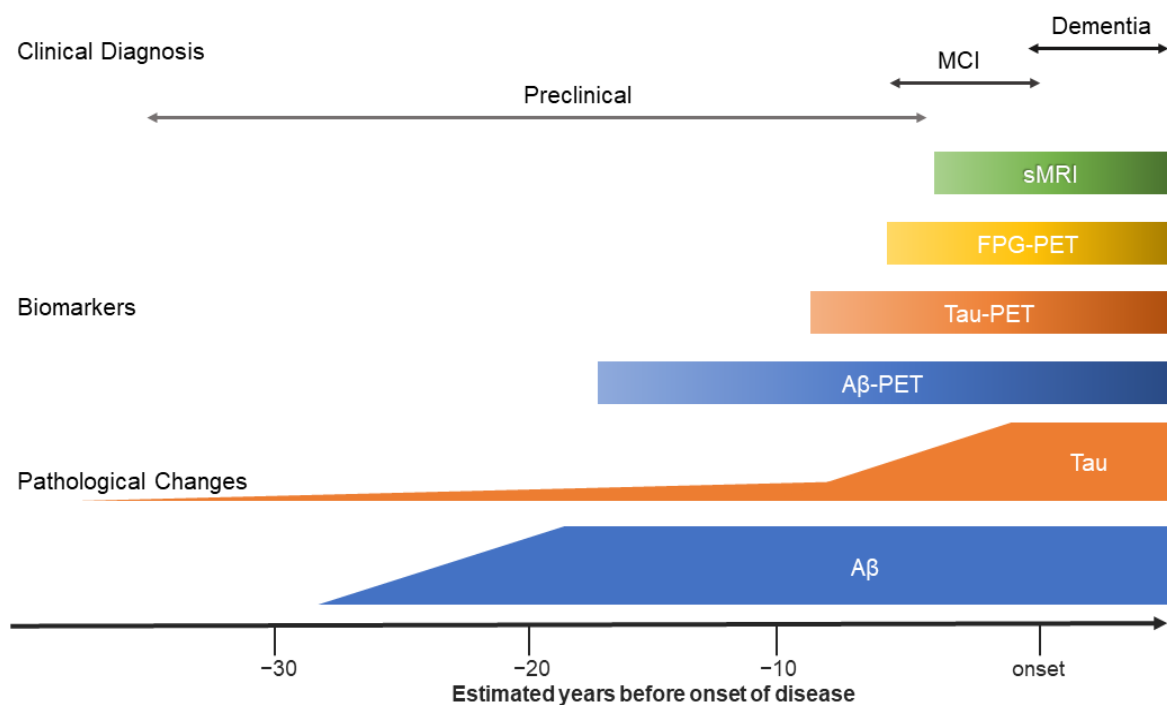


**Figure 1.** The Alzheimer's disease continuum with corresponding pathological changes, biomarkers and clinical diagnosis. Figure adapted from Yoshiyama et al. [21].

## 2. Contemporary Early Diagnosis of AD with Imaging Techniques

Since the number of patients with AD is increasing due to an aging population, much effort has been put into the detection of the disease as early as possible. Many methods have been tested, ranging from cognitive tests, MRI scans and sampling of cerebral fluid [22]. In this section, we focus on what imaging techniques and associated biomarkers are applied in the early diagnosis of AD.

The first applications of imaging techniques in AD were computed tomography (CT) and MRI, but these techniques were used to exclude other causes of dementia rather than to diagnose AD in an early stage [23]. Later, imaging techniques were utilized as positive support to confirm the clinical diagnosis of AD. These techniques focused on the neuronal injury and degeneration aspects of AD [1]. Nowadays, imaging modalities focus on either identifying amyloid deposition or identifying neurodegeneration [24].

### 2.1. Structural MRI

#### 2.1.1. Background

The pathology of AD follows a typical spreading pattern through the brain in which certain areas are among the first affected, while other regions will only be impaired in severe stages of AD [3,25]. In this so-called topographic pattern that characterizes AD, the earliest changes are found in the medial temporal lobe structures, the entorhinal and perirhinal cortex and the hippocampus [16] (Figure 2). This typical pattern of disease progression opened possibilities for the early diagnosis of AD by investigating these brain parts with imaging techniques.

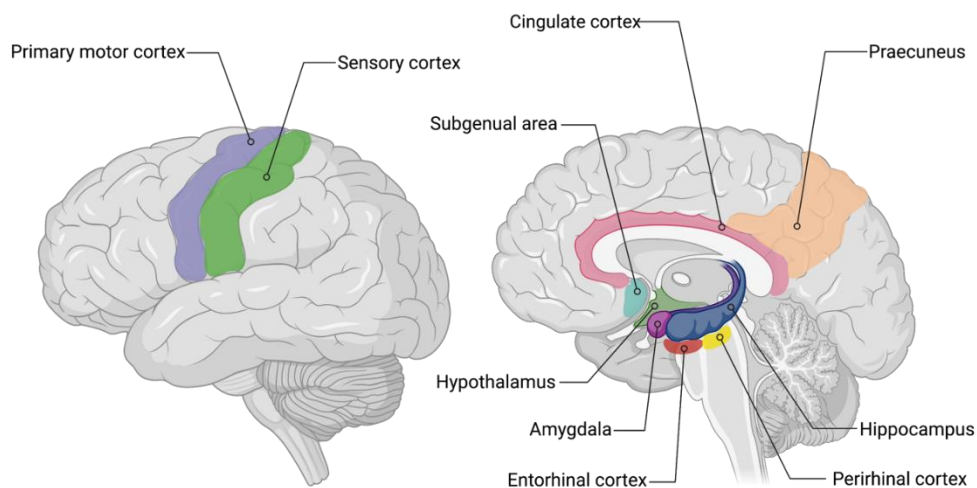


**Figure 2.** Regions affected by Alzheimer's disease. Figure created with [www.BioRender.com](http://www.BioRender.com) (accessed on 12 February 2021).

### 2.1.2. Findings

Since neuronal damage in the hippocampus is manifested as decreased hippocampal volume [26], a widely accepted method for assessing AD pathology is volumetric MRI scans of the hippocampus (Figure 3) [25]. These scans are T1-weighted images from which hippocampal atrophy can be measured with either manual or automated segmentation [27]. According to a study of Bobinski et al., MRI provided a powerful tool in assessing the hippocampal volume and predicted volumes that correlated strongly with neuronal numbers, suggesting the anatomic validity of volumetric MRI measurements [28]. Moreover, another study found that volume reductions in the hippocampus are early indications for AD pathology, measurable with MRI [29].

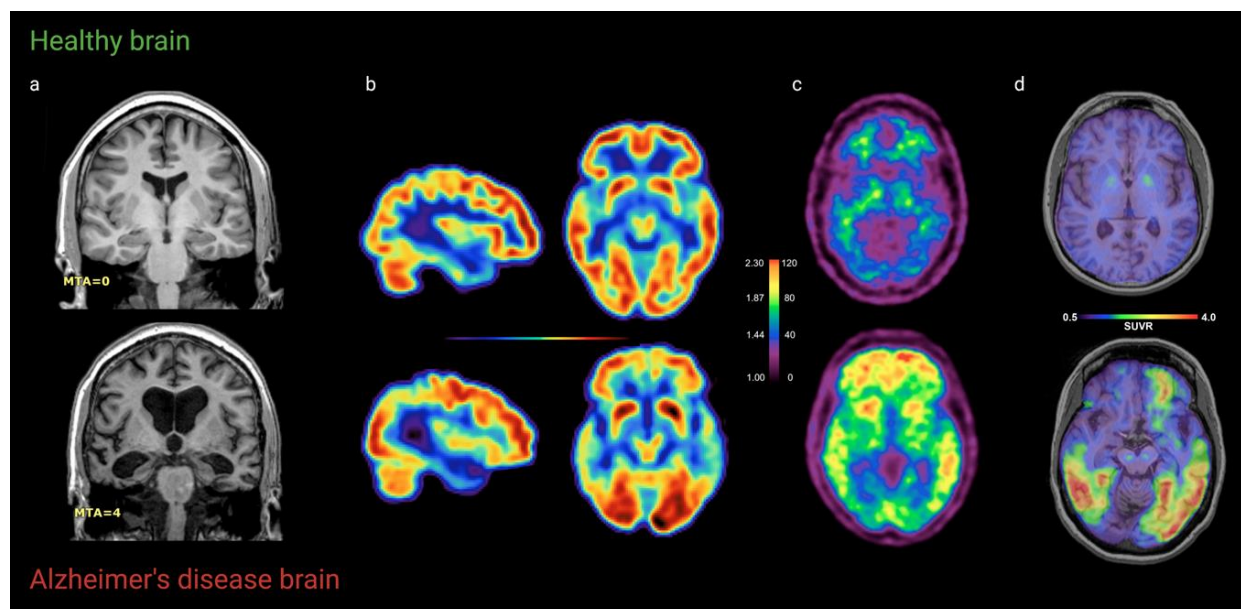


**Figure 3.** Neuroimages of the healthy versus the Alzheimer's disease (AD) brain. Neuroimaging with (a) structural MRI, (b) FDG-PET, (c) amyloid-PET with PiB and (d) tau PET with  $^{18}\text{F}$ -AV1451 in both healthy and AD brains. Figure created with [www.BioRender.com](http://www.BioRender.com) (accessed on 14 February 2021).

In addition to the hippocampus, other limbic brains regions that can be studied with MRI are the entorhinal cortex and amygdala (Figure 2). Although it is believed that the entorhinal cortex is among the regions affected first in AD [30–32] and the accuracy

of entorhinal cortex volumetry being slightly higher [32], several cross-sectional studies suggested that entorhinal cortex measurements are unlikely to offer additional benefits over hippocampal volumetry in AD patients when compared to healthy controls [33–35]. Moreover, high variability in methods to assess the entorhinal cortex volume due to anatomic ambiguity in the cortex's boundaries eliminates the slight superiority of the entorhinal cortex over the hippocampus [29,34,36].

In addition to the use of structural MRI in assessing volume reductions, another application of this imaging technique is to detect cortical thickness reduction in certain brain areas, such as the temporal, orbitofrontal and parietal regions [37]. Detailed study has demonstrated the effect of AD on cortical thickness and led to the suggestion of a so-called AD “disease signature” in which certain brain regions known to be affected by AD show cortical thinning [38]. Assessment of the cortical thickness is believed to be a useful biomarker in the early diagnosis of AD, since subtle changes in areas known to be affected by AD can be detected [39]. Furthermore, a study into region- and phase-specific changes has linked disease severity to cortical thickness [40], thereby coupling the clinical dementia ranking stages to a level of cortical thinning. Additionally, cortical thickness correlates strongly with cognitive impairment in the clinical stages of AD [41,42].

Over time, volumetric MRI of the hippocampus has been seen to be the best-established biomarker for AD [1,33,36,43], especially as a diagnostic marker in the mild cognitive impairment stage (MCI) [44]. Additionally, one major benefit of MRI is the availability of appliances in hospitals and research centres [23]. Moreover, MRI is safe and is seen as non-invasive, since it involves no ionizing radiation.

### 2.1.3. Limitations

However, structural MRI as an imaging technique for AD has its limitations. First, decreased hippocampal volume is not an AD-specific measure [14]. An extensive study by Geuze et al. reviewed more than 420 records reporting the assessment of hippocampal volume with MRI [45]. In addition to AD, other neurodegenerative diseases are characterized with diminished hippocampal volume as well such as Parkinson's disease [46], epilepsy [47] and Huntington's disease [48]. Additionally, volume reduction has also been observed after cardiac arrest [49], chronic alcohol abuse [50] and survivors of low birth weight [51]. Moreover, recent study has demonstrated that hippocampal texture predicts conversion from MCI to AD with higher accuracy than the hippocampal volume, although these results have to be validated with histological data [52]. Lastly, manual segmentation of T1-weighted images is time-consuming [53], requires specialistic training and can result in high levels of variability in the measurements [54], due to different protocols for assessing the measurements [33]. Fortunately, in the last decade, much effort has been put into establishing methods for automated segmentation, resulting in more accurate data from MRI images in less time [53,55–57]. One major drawback of structural MRI in general is the impossibility to directly observe the effect of amyloid plaques or NFTs in the brain. Atrophy is downstream of the pathological event and not disease specific [23]. Moreover, several studies demonstrated that in atypical forms of AD, the hippocampus is spared [58,59]. Therefore, structural MRI in atypical manifestations of AD might be not able to identify the disease in an early stage.

## 2.2. FDG-PET

### 2.2.1. Background

Multiple diseases affecting the central nervous system (CNS) are associated with impaired glucose uptake by neurons [60]. With fluorodeoxyglucose positron emission tomography (FDG-PET), it is possible to measure the resting state cerebral metabolic rates of glucose as a proxy of neuronal activity, without the requirement of cognitive activity [61,62]. FDG-PET measures the uptake of a radiolabeled glucose analogue which correlates with cerebral metabolism and synaptic activity (Figure 3) [23,43]. Since reduced cerebral metabolism is associated with age, healthy age-matched individuals show cor-

responding cerebral metabolism patterns [62]. The comparison of FDG-PET scans of AD patients with healthy individuals of the same age revealed patterns of metabolic abnormalities in AD, leading to a so-called FDG-PET endophenotype [23]. This endophenotype is seen as a characteristic of AD in which certain brain regions or areas are affected in a spatial pattern [24]. In AD, hypometabolism occurs first in the temporoparietal areas of the brain, including the precuneus and posterior cingulate cortex [1,61] (Figure 2). Moreover, as the disease progresses, the metabolic deficits are gradually aggravated [23].

### 2.2.2. Findings

Among the first studies that successfully applied FDG-PET in studying Alzheimer's disease was a research project by Benson et al. in 1983 in which both AD patients and patients with multi-infarct dementia were studied [63]. The results from this study revealed that in AD patients, almost all brain areas demonstrate reduced glucose metabolism, but the primary motor and sensory cortex are spared. This work inspired other researchers and led to an increase in studies investigating the effect of AD on glucose metabolism in the brain [64–66]. However, all these studies used patients with diagnosed AD in mild to severe stages of the disease and did not use FDG-PET to diagnose the patients.

In the 1990s, automated methods to standardize the evaluation of PET scans increased, leading to more consistency in the evaluation of FDG-PET images obtained in different research centers or with different equipment [67,68]. A large study by Silverman et al. used FDG-PET as a diagnostic tool for differentiating healthy individuals from patients with AD symptoms. In the study, the sensitivity and specificity of FDG-PET were addressed, in which sensitivity reflects the ability to identify AD subjects among all individuals, whereas specificity addresses the ability to correctly identify subjects as non-AD. FDG-PET was able to detect AD subjects with a sensitivity of 94% and a 73% specificity. Additionally, in patients diagnosed with questionable or mild dementia, the sensitivity was 95% with a specificity of 71% [69]. These results indicated that FDG-PET is a sensitive indicator of AD and can also be used to assess early-stage dementia. The findings were underlined with other research studies with sensitivity ranging from 84% to 93% and specificity between 63% and 74% [70,71]. Furthermore, reviews based on meta-analyses of articles regarding the identification of AD patients among healthy individuals resulted in pooled sensitivities up to 96% with specificities up to 90% [72–74]. Finally, Panegyres et al. demonstrated that FDG-PET is able to differentiate between different types of dementia up to 95% [60].

Over the years, FDG-PET emerged to be a relevant and highly specific biomarker for the early diagnosis of AD and other types of major neurodegenerative diseases [43,75]. It is seen as a robust and reliable biomarker in the *in vivo* diagnosis of early stages of AD [23,36,43]. Moreover, compared to structural MRI of the hippocampus and entorhinal cortex, FDG-PET is diagnostically superior to volumetry measures [76]. Additionally, according to the hypothetical model of dynamic biomarkers proposed by Jack and colleagues, abnormal FDG-PET precedes changes detectable with MRI [77,78] (Figure 1), suggesting an FDG-PET of higher value than structural MRI in the early diagnosis of AD.

### 2.2.3. Limitations

However, FDG-PET has its limitations. PET scanners are not widely available and considered as relatively expensive [23,36]. FDG-PET requires the intravenous injection of a radiolabeled agent and is, therefore, more invasive than MRI. Moreover, hypometabolism is a result of neurodegeneration and, therefore, it might not be suitable to detect signs of AD in the earliest stages before neuronal loss occurs [79]. By the time hypometabolism is measurable with FDG-PET, damage inflicted to neurons might be too severe to benefit from therapies. Additionally, increasing evidence suggests that FDG-PET shows the consumption of glucose by astrocytes, rather than by neurons and, therefore, hypometabolism can be ascribed to decreased astrocyte function [80]. Lastly, it is important to keep in mind that atypical clinical manifestations of AD may have the same pathophysiology as typical AD, but can show distinct metabolic patterns [81]. This heterogeneity in changes in metabolic

patterns among the distinct AD subtypes can reduce the diagnostic accuracy of FDG-PET. Since neurodegeneration is a pathological event preceded by amyloid plaques and NFTs, biomarkers sensitive for these two events might be more suitable for the diagnosis of AD in the early stages than FDG-PET.

### 2.3. Amyloid-PET

#### 2.3.1. Background

Many researchers believe that the first pathological event in AD is A $\beta$  accumulation, leading to the formation of senile plaques [7,20,82,83]. However, this belief is still subject to debate [84,85]. To detect and design therapies for plaques, it is important to find out what causes plaque formation. Therefore, senile plaques were intensively studied, but due to their insolubility, the attempts to identify their composition in many studies failed [12]. Finally, in the mid-1980s, researchers were able to identify the A $\beta$  protein as a primary component of the plaques. This protein, with an average chain length of forty-two amino residues, results from the cleavage of the larger amyloid precursor protein (APP) by  $\beta$ - and  $\gamma$ -secretase (Figure 4) [36,86]. At first, it was believed that A $\beta$  was an abnormal protein, but the presence of A $\beta$  in culture medium, cerebrospinal fluid (CSF) and plasma revealed that A $\beta$  is a normal product of APP metabolism [12,83]. This understanding led to a new hypothesis: the amyloid cascade hypothesis. This hypothesis states that a dysregulation in the production and clearance of A $\beta$  in the brain leads to the accumulation of A $\beta$  in oligomers, protofibrils and eventually mature fibrils [87], ultimately leading to neurodegeneration and dementia. All other disease characteristics, such as the formation of NFTs out of hyperphosphorylated tau, and neurodegeneration, are seen a result of this accumulation [12,83,88].

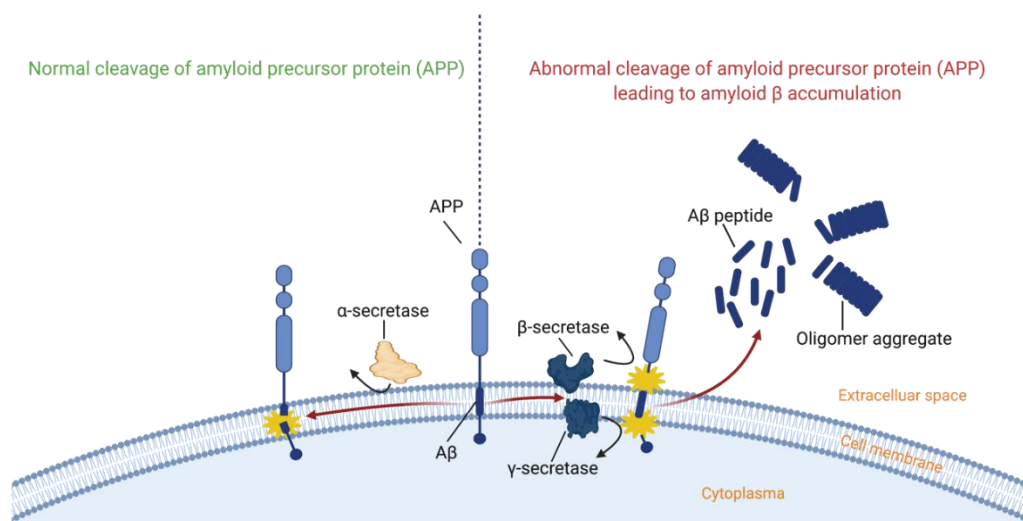


**Figure 4.** Accumulation of amyloid- $\beta$  in AD. Figure adapted from Patterson et al. [89] and created with [www.BioRender.com](http://www.BioRender.com) (accessed on 16 November 2020).

#### 2.3.2. Findings

Because A $\beta$  deposition in the brain is commonly seen as the earliest hallmark of AD, many studies have focused on identifying biomarkers that differentiate healthy controls from individuals with the first pathophysiological signals of AD. Currently, two distinct biomarkers are used to assess A $\beta$  pathology: the concentration of A $\beta$ 42 in the CSF and amyloid-PET [1,77,90]. In this section, we discuss how PET imaging of the A $\beta$  accumulation can contribute to the early diagnosis of AD.

### <sup>11</sup>C-PiB

In 2004, a novel <sup>11</sup>C radiotracer named Pittsburgh compound-B (PiB) was applied in a study containing mild AD patients and a control group [91]. The study showed that PiB retention time was equivalent in both groups in brain regions known to be relatively unaffected by A $\beta$  deposits. However, compared to controls, the individuals with mild AD showed considerable retention of PiB in areas known to contain substantial A $\beta$  accumulation in AD (Figure 3). These areas included cortical areas, such as the frontal cortex and neocortex (Figure 2). The findings suggested that PET neuroimaging with PiB could provide quantitative information about A $\beta$  deposition in living patients in early (mild AD) stages of the disease.

Rabinovici et al. demonstrated that amyloid-PET imaging with PiB was able to distinguish AD subjects from patients with other forms of dementia, such as frontotemporal dementia (FTD) [92]. All AD subjects (7/7) had positive PiB-PET scans, while in FTB patients and healthy controls, respectively, 8/12 and 7/8 scans were negative. These findings were confirmed in a study with AD subjects and patients suffering from FTD in which the retention time of PiB in FTD patients was measured. In total, 8/10 FTD patients showed a significantly lower retention time compared to AD subjects, indicating that PiB might be a tool in differentiating FTD from AD [93].

In addition to differentiating between different types of dementia, amyloid-PET with PiB was able to identify the different stages of the AD continuum. In a study by Lowe et al., PiB-PET was able to significantly differentiate healthy controls from non-amnesic MCI and amnesic MIC, and AD [94]. In another study, PiB-PET clearly differentiated AD patients from MCI and healthy subjects [95]. Moreover, both studies suggested that the diagnostic value of PiB-PET increases when combined with FDG-PET, since information obtained from both techniques might be complementary. In 2014, Leuzy et al. published a paper concerning the increased PiB retention restricted to specific brain regions associated with higher levels of A $\beta$  deposition [96]. This pattern was histological confirmed by the comparison of imaging data with immunohistochemical exams post-mortem [97,98].

On a molecular level, PiB is believed to bind insoluble A $\beta$  fibrils [99]. Another study reports the strongest PiB binding to A $\beta$ 42 fibrils, followed by significant binding to A $\beta$ 42 oligomers and protofibrils [100], but compared to the fibril binding, this binding to protofibrils and oligomers is increasingly lower. Additionally, increasing evidence suggests insoluble A $\beta$  being only a fraction of total A $\beta$  in the brain [101] and a more prominent role of soluble protofibrils in the pathogenesis of A $\beta$  [102]. A $\beta$ -Pet with PiB may, therefore, be more a reflection of a fraction of insoluble A $\beta$  than an image of total A $\beta$  pathology in the brain.

Over the years, amyloid-PET with PiB has emerged as the gold standard in A $\beta$  imaging [86]. Nevertheless, PiB has its limitations and drawbacks as a radiotracer in A $\beta$  imaging. First, the short half-life (twenty minutes) of the <sup>11</sup>C isotope requires a nearby cyclotron for clinical usage [86,103]. Second, as previously mentioned, PiB has the tendency to only bind to the fibrillar form of A $\beta$  and has low affinity for soluble oligomeric A $\beta$  [104], while it is believed that in some genetic forms of AD, oligomeric A $\beta$  plays a significant role in the disease manifestations [105,106]. PiB-PET might fail as a diagnostic tool in identifying these types of AD. Lastly, the selectivity of a positive A $\beta$  scan obtained with PiB as a biomarker for AD is relatively low, because elevated PiB uptake has also been found in 30% of healthy controls without cognitive disorders [4].

### <sup>18</sup>F-Labelled Radiotracers

The short half-life of <sup>11</sup>C in PiB led to the development of <sup>18</sup>F-labelled radiotracers, and in 2008, the first study reported successful imaging with a fluorinated radiotracer in humans [107]. Currently, three <sup>18</sup>F-labelled radiotracers for assessing A $\beta$  deposition are approved: florbetapir, flutemetamol and florbetapen [86]. Florbetapir was the first fluorinated radiotracer and had retention ratios strongly associated with PiB [103,108]. A detailed meta-analysis into the three <sup>18</sup>F-labelled radiotracers revealed no apparent

differences between the diagnostic accuracy of the radiotracers [109]. However, compared to PiB, the fluorinated tracers showed higher levels of non-specific uptake in the white matter due to the more lipophilic nature of both radiotracer and white matter [110,111], resulting in more background noise [112]. Due to this extra noise, the typical white matter pattern caused by cortical amyloid plaque is lost [113].

### 2.3.3. Limitations

Altogether, A $\beta$ -PET collected the first in vivo evidence of earliest protein deposition [114]. PET has become a powerful tool in the detection of A $\beta$  deposition and can contribute to the early diagnosis of AD. However, to fully employ its opportunities, some obstacles must be resolved. One difficulty to overcome is finding a consensus on methods to quantify amyloid-PET scans [86]. There is an urgent need for a tool to discover even the smallest A $\beta$  deposits, and cut-off levels need to be defined in order to make studies comparable [4]. Furthermore, most studies have used radiolabeled tracers in the typical form of the AD spectrum, resulting in much knowledge about A $\beta$  accumulation in typical AD, while the atypical, non-amnesic type has remained understudied [115]. An increasing body of evidence suggests the utility of A $\beta$ -PET to diagnose patients with atypical manifestations of AD, such as posterior cortical atrophy (PCA) and logopenic-variant primary progressive aphasia (LvPPA) [104,116]. To maximally benefit from the diagnostic accuracy of A $\beta$ -PET, more study into A $\beta$  accumulation in atypical subtypes of AD is required. Lastly, the amyloid cascade hypothesis is still a hypothesis, and although A $\beta$  deposition is an early event in the pathogenesis of AD, it may not be the direct cause of neurodegeneration and cognitive decline [86].

## 2.4. *Tau-PET*

### 2.4.1. Background

Since multiple attempts for developing anti-amyloid drugs have failed in clinical trials, interest has shifted from treating A $\beta$  accumulation towards development of PET radiotracers for identifying tau aggregates. This shift of interest is accompanied by the thought that tau protein aggregates are more closely related with cognitive impairment [111,117]. Furthermore, increasing evidence suggests a role for oligomeric A $\beta$  and tau species in the early stages of AD rather than A $\beta$  plaques and NFTs [118,119]. Tau is a microtubule-associated protein with six isoforms and is abundantly expressed in the CNS where it stabilizes the microtubules of axons (Figure 5) [120]. Several posttranslational processes can modify tau, such as acetylation, glycosylation, methylation and phosphorylation, which affect the ultrastructural conformation of tau [121]. Although normal phosphorylation of tau is required for its role in cytoskeletal plasticity during early development [122], hyperphosphorylation combined with decreased dephosphorylation leads to soluble hyperphosphorylated tau [123] that rapidly aggregates into so-called tauopathies [124]. In AD, aggregation of tau results in paired helical fragments (PHFs), and these PHFs can further accumulate into intracellular NFTs [117,123]. Even though the exact mechanism of tau aggregation is still unclear, the accumulation of tau is considered to play a major role in the neurodegenerative aspect of AD [7].

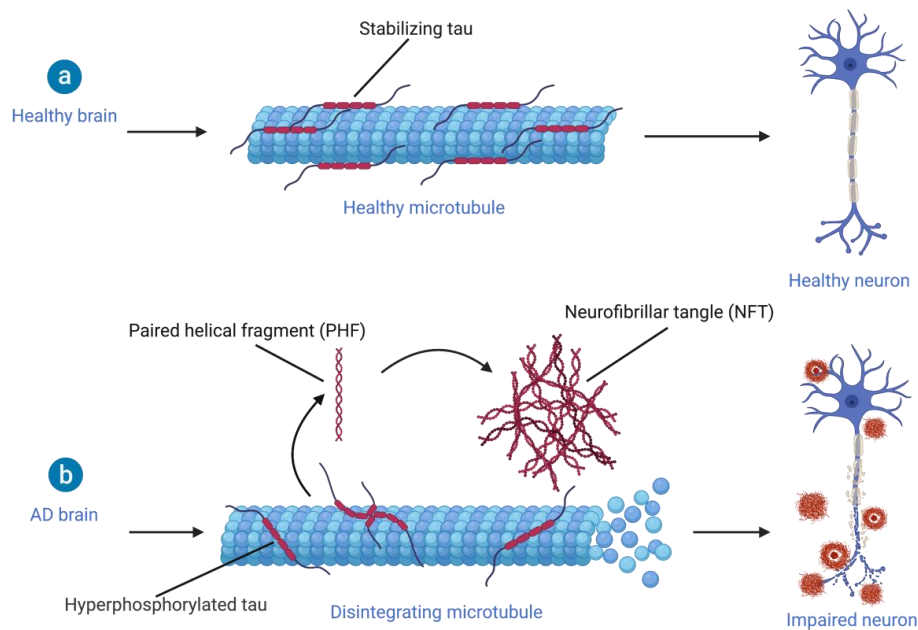


**Figure 5.** Tau protein aggregation leads to formation of neurofibrillary tangles in AD. (a) Role of tau protein in healthy brain; (b) role of tau protein in Alzheimer's disease brain. NFT: neurofibrillary tangles; PHF: paired helical filaments. Figure adapted from "Pathology of Alzheimer's Disease", by BioRender.com (2020). Retrieved from <https://app.biorender.com/biorender-templates> (accessed on 16 November 2020).

#### 2.4.2. Findings

Just like A $\beta$  accumulation, NFTs spread through the brain as AD progresses. This spreading pattern initiates in the entorhinal cortex (Figure 2), and as the disease progresses, NFTs spread to the limbic (stage III-IV) and isocortical (V-VI) association areas (Figure 6) [124]. However, in atypical variants of AD, the exact spreading pattern may be distinct from typical AD, and these differences in spreading patterns characterize atypical variants in early stages [125]. Although post-mortem quantification of tauopathies in the brain remains the gold standard, growing evidence suggests a role for tau-PET imaging with radiotracers *in vivo* for the clinical evaluation of the disease [124,126]. There are several challenges in the development of radiotracers for tau-PET. First of all, PET tracers must be able to pass the blood-brain barrier (BBB) [117]. Second, the intracellular location of NFTs poses a second barrier for the radiotracer to overcome [4,117,127]. Moreover, rapid clearance from the blood and high sensitivity are desired [117]. Since A $\beta$  deposits and NFTs both compromise beta sheets and A $\beta$  concentrations are remarkably higher, high affinity for tau over A $\beta$  is required [123].

In AD, tau aggregates are most prominently present in the ultrastructural PHF form and therefore most attempts in developing tau-PET tracers have focused on imaging these PHFs [127]. Based on their structures, the currently available tau tracers can be divided into four groups: the nonselective tracer  $^{18}\text{F}$ -FDDNP, quinoline derivatives, pyrido-indole derivatives and PBB3 [123,124]. Computational modeling of tau fibril using cryo-EM structures of PHFs and straight filaments [128] has identified four high-affinity binding sites for tau tracers [129]. Three binding sites are buried within the core of the fibril, whereas one site is located on the surface. The next section discusses several tau PET tracers and their binding to tau at the molecular level based on this computational model.

#### $^{18}\text{F}$ -FDDNP

$^{18}\text{F}$ -FDDNP is a fluorinated naphthyl-ethylidene derivative and was the first tracer applied in PET imaging of tauopathy in the brain [130]. This tracer is able to bind both extracellular amyloid- $\beta$  plaques and intracellular NFTs due to the presence of  $\beta$  sheets

in these proteins [131,132].  $^{18}\text{F}$ -FDDNP seems to favor the core sites of the tau fibril for binding [129] due to hydrophobic interactions. In addition to  $\text{A}\beta$  plaques and NFTs,  $^{18}\text{F}$ -FDDNP also binds prion plaques and is used to assess chronic traumatic encephalopathy suspicion [127,130]. Since  $^{18}\text{F}$ -FDDNP favors binding to amyloid- $\beta$  over tau [127,129,132], screening of  $\beta$  sheet-binding small molecules was performed on a large scale to identify more suitable and specific tau tracers.

#### Quinoline Derivatives

The first selective tau PET tracers were based on quinoline and benzimidazole derivatives [111,133] and focused on the imaging of PHF tau [127]. A study by Okamura et al. synthesized three new compounds, BF-126, BF-158 and BF-170, as possible probes for in vivo tau-PET imaging in the brain [133]. The compounds showed good brain uptake combined with rapid clearance from brain tissue. Additionally, in the neuropathological exam, the three compounds were able to visualize NFTs and PHF-type neuritis, suggesting that quinoline and benzimidazole derivatives might be potential tracers for tau-PET. With these findings in mind, the search for selective tau tracers continued with the development of  $^{18}\text{F}$ -THK5105 and  $^{18}\text{F}$ -THK5117. These two compounds were developed to enhance the binding affinity to PHF-tau [7] and demonstrated binding affinity and selectivity to PHF-tau over amyloid- $\beta$  in AD [134]. Similar to  $^{18}\text{F}$ -FDDNP, these two radiotracers favor the hydrophobic core sites of tau over the surface site according to the computational model [129]. Moreover, clinical PET studies revealed that these radiotracers were able to differentiate brains of AD subjects from brains of healthy controls [135,136]. A drawback of these radiotracers was the high non-negligible binding to white matter caused by the  $\beta$  sheet conformation of myeline. To solve this problem,  $^{18}\text{F}$ -THK5351 was developed. This new compound exhibited rapid clearance from the white matter [137]. Additionally,  $^{18}\text{F}$ -THK5351 showed higher specific binding to tau-associated regions than  $^{18}\text{F}$ -THK5117 [138]. As a result,  $^{18}\text{F}$ -THK5351 occurs to be the most promising arylquinoline radiotracer for the early detection of tau-associated pathology in AD subjects [111].

#### Pyrido–Indole Derivatives

$^{18}\text{F}$ -T808 and flortaucipir, also known as  $^{18}\text{F}$ -AV-1451 or  $^{18}\text{F}$ -T807, are both fluorinated pyrido-indole derivatives with high selectivity for tau over  $\text{A}\beta$  deposits [4,111]. Although  $^{18}\text{F}$ -T808 exhibited high tau affinity, rapid uptake and clearance, a disadvantage of this compound was de defluorination followed by bone uptake of  $^{18}\text{F}$  [139]. On the other hand, flortaucipir showed over 25-fold selectivity for tau against  $\text{A}\beta$  plaques combined with low levels of white matter uptake [4]. Moreover, the uptake of flortaucipir corresponds well with the expected spatial pattern of tau pathology in the brain of AD subjects (Figure 3) [140,141]. Furthermore, it is believed that flortaucipir binds with high affinity to all three isoforms of tau when in the classical PHF form [142], which is likely due to its high affinity for more than one binding site of the tau fibril [129]. However, flortaucipir exhibited low affinity for tau aggregates consisting of primarily straight tau filaments (Figure 5), indicating that flortaucipir might not be a suitable radiotracer in diseases other than AD.

#### PBB3

The last group of tau-PET tracers consists of PBB3, a  $^{11}\text{C}$ -labelled radiotracer that is able to detect both AD and non-AD tauopathies [132]. The compound exhibited up to 50-fold higher binding affinity for tau than for  $\text{A}\beta$ , binds to a wide range of tau isoforms [143] and has affinity for tau at a binding site differently than other radiotracers, which might explain its wide binding range [129]. The uptake of the compounds is elevated in the hippocampus and spreads to the association cortex as disease progresses. The drawbacks of PBB3 are the usage of short half-life  $^{11}\text{C}$  in the radiotracer and the ability of its major metabolite to cross the BBB [143,144].

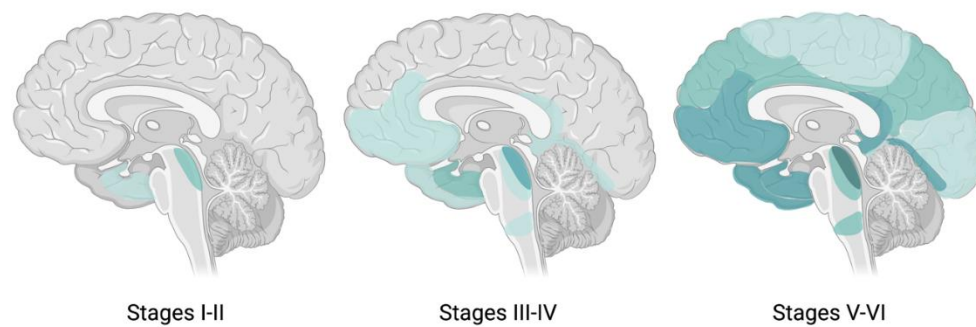


**Figure 6.** Tau spreading pattern in each Braak stage. Spreading pattern of tau throughout the brain from Braak stage I-II to stage III-IV (limbic regions) and stage V-VI (isocortical areas). Figure adapted from Goedert [145] and created with [www.BioRender.com](http://www.BioRender.com) (accessed on 11 February 2021).

#### 2.4.3. Limitations

The development of novel tau tracers is an ongoing process in which several pharmaceutical companies are trying to improve the pharmacokinetics and pharmacodynamics of the tracers [7]. Compared to  $A\beta$ , the development of tau-PET tracers is still behind, and clinical validation of the tracers is required [146]. Nevertheless, tau-PET poses another neuroimaging tool for the early diagnosis of AD.

#### 2.5. Summary

Although the applications of imaging techniques in the early diagnosis of AD are on the rise, an impeccable biomarker that can diagnose AD in the earliest stage is still not available. All current techniques have their limitations (Table 1), and most importantly, there is a significant amount of protein deposition or atrophy needed for detection. Since AD is known to have decades of pathological changes before the clinical onset of disease and disease-modifying treatments may be the most beneficial before certain thresholds of protein levels or atrophy are passed, current imaging biomarkers may diagnose AD in an overly progressed stage in which therapies will inevitably fail.

**Table 1.** Advantages and limitations of imaging techniques currently used in early diagnosis and longitudinal monitoring of AD.

Technique	Early Diagnosis	Longitudinal Monitoring
Structural MRI	Advantages	Powerful in predicting volumes Changes in atrophy closely related to changes in cognitive abilities High atrophy rates predict cognitive decline
	Limitations	MRI scanners widely available Safe Decreased hippocampal volume not AD-specific measure Atrophy patterns differ among AD subtypes
FDG-PET	Advantages	Extensive research led to an FDG-PET endophenotype usable for comparison Highly sensitive and specific Differences in metabolism patterns able to predict risk to convert to AD Diminished FDG uptake precedes clinical manifestation Heterogeneity in topographic progression of reduced metabolism may predict AD variant
	Limitations	Reduced glucose metabolism caused by other diseases or injuries Rather reflection of glucose consumption by astrocytes Invasive due to injection and radiolabelled tracer Expensive and not widely available

Table 1. Cont.

Technique	Early Diagnosis	Longitudinal Monitoring
Amyloid-PET	Advantages	<p>A<math>\beta</math> plaques seen as earliest hallmark of AD</p> <p>Retention time of radiotracers matches spreading pattern of A<math>\beta</math> plaques</p> <p>PiB retention time able to predict conversion from MCI to AD</p>
	Limitations	<p>Exact role of A<math>\beta</math> accumulation in AD still unknown</p> <p>Elevated PiB uptake also found in healthy controls</p> <p>No standard method for quantifying A<math>\beta</math> plaques</p> <p>Not much known about A<math>\beta</math> accumulation in atypical forms</p> <p>Weak correlation between A<math>\beta</math> deposition and disease severity</p> <p>A<math>\beta</math> accumulation stabilizes in later stages of AD</p> <p>Choice of reference region subject to debate</p>
Invasive due to injection and radiolabelled tracer		
Tau-PET	Advantages	<p>Tau accumulation believed to be closely related to cognitive impairment</p> <p>Radiotracer uptake matches spreading pattern of tau</p> <p>Radiotracers have high affinity for PHF tau</p> <p>Strong relationship between neurofibrillary pathology and neurodegeneration</p> <p>Accumulation rates consistently increase throughout the brain</p>
	Limitations	<p>Most tracers low affinity for straight filaments</p> <p>High level of heterogeneity in tau topography between AD subtypes</p>
Still new field of research Invasive due to injection and radiolabelled tracer		

### 3. Contemporary Longitudinal Monitoring of AD with Imaging Techniques

Since AD is a progressive chronic disease with no clinical endpoint, the longitudinal monitoring of disease progression and variations in biomarker levels can give insight into the pathogenesis and prognosis of the disease [14]. In correspondence with the early diagnosis of the disease, to date, there is no consensus on the biomarkers, techniques or tests that are the most clinically relevant in monitoring the disease in the long-term. In this section, we discuss the imaging techniques and associated biomarkers that are applied in the longitudinal study of AD.

#### 3.1. Structural MRI

##### 3.1.1. Background

Whilst structural MRI might not be the most suitable technique for the early diagnosis of AD, many studies have used structural MRI to monitor disease progression, because rates of change in multiple structural measures are closely associated with changes in cognitive abilities [44].

##### 3.1.2. Findings

In an early study by Fox et al. in 1999, whole-brain atrophy was linked to increased disease severity [147]. Patients with untreated, probable AD were age-matched with a group of healthy controls to assess the relationship between disease severity and atrophy progression within the subject. Each individual underwent at least two MRI scans and both groups also participated in mini-mental state examinations (MMSE) on the MRI scans' dates. The scans revealed that AD subjects had a mean rate of whole-brain atrophy of  $2.4 \pm 1.4\%$  per year, while the control group had a mean loss of  $0.4 \pm 0.7\%$ . Additionally, the MMSE scores demonstrated a significant difference in the mean rate of decline between AD patients

and healthy individuals, indicating that rate of cerebral atrophy is strongly correlated with decline in cognitive ability. Two other studies also investigated the correlation between whole brain atrophy rates and cognitive performance and underlined the finding that whole-brain atrophy is strongly associated with cognitive decline, making cerebral atrophy an interestingly and clinically relevant biomarker for tracking AD progression [148,149]. Moreover, one of the studies implicated patients with MCI and found that a higher rate of brain atrophy per year was associated with an elevated risk of developing dementia [148].

In addition to whole-brain atrophy, rates of atrophy have also been evaluated in other structural regions of the brain. Cardenas et al. focused on identifying spatial patterns of brain atrophy associated with cognitive performance and possible future cognitive decline [150]. The study used deformation-based morphometry (DBM) in which every voxel is spatially normalized to a template brain. This enables the comparison between subjects with different rates of disease progression [36]. Atrophy rates in the hippocampus and entorhinal cortex (ERC) of non-demented elderly with different levels of cognitive performance were combined with several neuropsychological tests. Smaller volumes of hippocampus and ERC were strongly correlated with memory function at baseline and also predicted memory decline [150]. These results suggest that baseline volumes of these regions may predict cognitive decline due to aging, pathology or both.

Thompson et al. created maps of hippocampal and ventricular change over a longer period with a goal to visualize the spatial progression of AD and the rate of change [151]. Over time, the hippocampal volume decreased, while the ventricular volumes expanded (Figure 7). Interestingly, the spreading patterns were different between aging and dementia. Temporal horn expansion in the ventricles turned out to be a promising marker for disease progression and corresponded well with rates of cognitive decline. These results suggest that visualizations of hippocampal atrophy and ventricular expansion rates may provide a promising marker to monitor AD progression. In a study by Jack et al., the above structural MRI measures were combined and evaluated on their ability to predict disease progression [152]. A group of 160 individuals was recruited based on their profile to meet either the criteria for cognitively unimpaired, MCI or AD. All subjects had a series of MRI scans of the whole brain, hippocampus, entorhinal cortex and ventricles. Similar to the previously described studies, the change in cognitive performance was assessed with multiple tests. Over time, subjects could remain stable or shift to a more cognitive impaired group. In all brain regions, the atrophy rates were higher among subjects that converted to a more severe disease profile and supported the applicability of rates of change from longitudinal MRI measures as markers for AD progression.

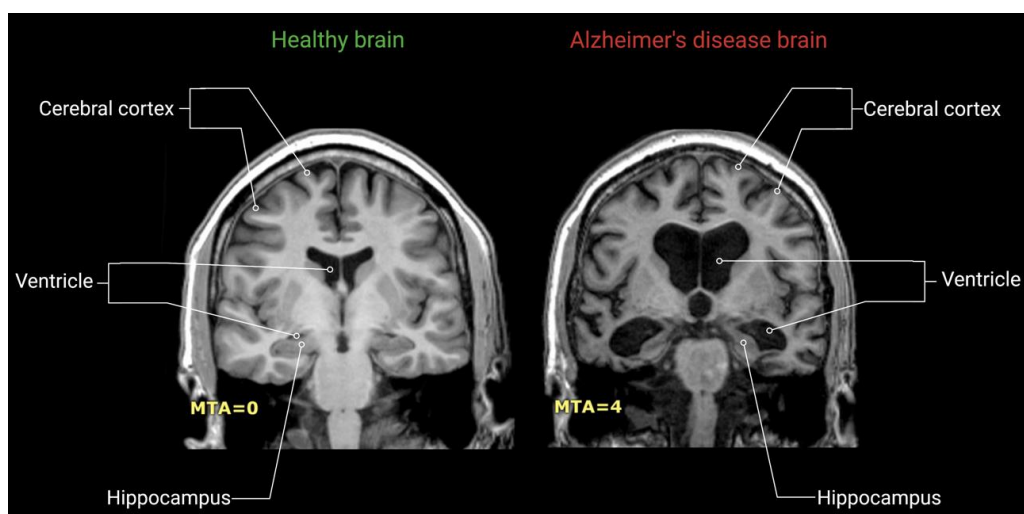


**Figure 7.** AD leads to hippocampal atrophy and ventricle enlargement. Healthy brain (left) versus AD brain (right). AD leads to decreased hippocampal volume, shrinkage of cerebral cortex and ventricle enlargement. MTA: medial temporal lobe atrophy; MTA = 0: no atrophy in medial temporal lobe; MTA = 4: severe volume loss of hippocampus. Figure created with [www.BioRender.com](http://www.BioRender.com) (accessed on 14 February 2021).

### 3.1.3. Limitations

Although from these results, changes in atrophy rates of several brain regions may seem promising for the longitudinal monitoring of AD, these methods also have their disadvantages. Lawrence et al. found that most studies that monitor disease progression have small sample sizes with regularly below a hundred participants, probably due to high costs associated with repeated MRI measures [14]. Additionally, there is a lack of studies that implement more than one follow-up scan, and most studies have limited time between the two scans, while AD progression is protracted. Furthermore, whole-brain atrophy rates and hippocampal volume reduction are not AD-specific measures, and since MMSE is not sensitive enough to diagnose AD [153], atrophy rates and declined cognitive performance might be wrongly attributed to AD. In similarity with sMRI in the early diagnosis of AD, it is important to note that spatial patterns of atrophy differ per AD subtype [58]. In typical AD, key regions of atrophy are the hippocampus and ERC, whilst in atypical AD, such as the previously mentioned LvPPA and PCA, but also the dysexecutive/behavioral variant [154], these regions undergo slower rates of change [58,59]. It is, therefore, important to discriminate between the different types of AD before longitudinal assessments of atrophy rates are made.

## 3.2. FDG-PET

### 3.2.1. Background

In the previously reported study of Panegyres et al., FDG-PET was listed as a promising technique in the early diagnosis of AD and other types of early-onset dementia [60]. Although in this study, longitudinal clinical follow-up was included, this was primarily conducted as a diagnostic reference standard [74]. There are, however, other studies that have assessed the clinical relevance of FDG-PET as a tool for disease progression in AD.

### 3.2.2. Findings

The first study to longitudinally monitor changes in metabolism patterns with FDG-PET was a follow-up study by Drzezga et al. in 2003. MCI subjects underwent two FDG-PET scans with an interval of one year to identify typical patterns of cerebral metabolism [155]. Since patients suffering from MCI have a high risk to convert to AD within one year, FDG-PET scans of these MCI patients may give insight into the pathophysiology of AD. Converter MCI patients showed decreased glucose metabolism in the temporoparietal and posterior cingulate cortex at baseline (Figure 2). After one year, the glucose metabolism also decreased in prefrontal areas, along with a further diminished metabolism in the posterior cingulate cortex, while these regions were spared in stable MCI patients. The results indicated that metabolic change rates within one patient group can differ over time as disease progression differs. Differences in cognitive decline are correlated to different spatial patterns of decreased glucose metabolism and can be used to predict one's risk to convert to AD.

Fouquet et al. expanded this study by also taking into account the metabolic characteristics that distinguish converters to AD from stable MCI patients [156]. Amnesic MCI (aMCI) patients were recruited and had two FDG-PET scans with an eighteen month interval. All aMCI subjects had progressive metabolic decline over the follow-up period in the temporoparietal cortex and posterior medial parietal areas. Moreover, two medial prefrontal areas, i.e., the anterior cingulate cortex and subgenual area (Figure 2), had significantly greater decline in converters than stable aMCI subjects. This contrasts with the findings of Drzezga et al., in which lateral prefrontal regions were areas of hypometabolism. However, multiple studies support the assumption of Fouquet et al., reporting decreased metabolism in the same two medial prefrontal regions [3,157] Altogether, these findings highlight the potential of FDG-PET for the longitudinal monitoring of AD progression.

The previously described studies did not discriminate between patients with early and late MCI. This distinction in the MCI stage has been proposed by Alzheimer's Disease Neuroimaging Initiative (ADNI), a consortium focusing on the development of standard-

ized biomarker procedures and use of imaging techniques in healthy, MCI and mild AD subjects [158]. The ADNI criteria classify subjects into MCI based on the scores from different tests, such as MMSE, WMS-R Logical Memory II and Clinical Dementia Rating (CDR). Classification into early MCI or late MCI is solely based on the outcome of the WMS-R Logical Memory II test, and the ADNI refers to early MCI subjects as patients that meet all the criteria for aMCI, but are in an earlier, and, therefore, less severe, point on the clinical spectrum [158,159]. With this discrepancy in mind, another research project focused on investigating differences in hypometabolism patterns and neuropsychological characteristics between early and late MCI [160]. Evaluation of the baseline scans and tests with the follow-up tests suggested that early MCI patients differ in patterns of hypometabolism and associated cognitive deficits compared to late MCI subjects. A major limitation of this study is the inclusion of only one FDG-PET scan at baseline instead of scans at every follow-up to track hypometabolism progression. There are several more studies that have identified FDG-PET as a promising tool to predict one's risk to convert from cognitively unimpaired to MCI and from MCI to AD [161–164]. In a more recent study, patients already converted to AD were followed for three years to observe longitudinal changes in cortical glucose metabolism in amnesic and non-amnesic subjects with sporadic AD [165]. FDG-PET images at baseline demonstrated different regions with diminished glucose metabolism in amnesic and non-amnesic subjects. Similar progression patterns of metabolic reduction were observed in most regions, except for a higher rate of decline in anterior cortices in non-amnesic forms. Glucose decline progressed from anterior to posterior in amnesic patients, while in non-amnesic subjects, decline progressed along a posterior-to-anterior axis. Additionally, the non-amnesic early-onset AD patients presented more rapid and severe decline in glucose metabolism than amnesic subjects. The differences found in the spatial distribution and temporal trajectory of hypometabolism between amnesic and non-amnesic early-onset AD suggested the treatment of these two forms of sporadic AD as two separate entities. A limitation of this study was the high amount of attrition due to disease severity at baseline, which is a characteristic of early-onset AD.

Ishibashi et al. recruited healthy individuals from an ongoing longitudinal study of cognition and aging. These controls were compared with two female subjects that were diagnosed with AD during the study and with a group of fifteen patients in the early stage of AD [166]. Female subject A had a glucose reduction rate of 9.41% over nine years, whereas female subject B's glucose metabolism decreased with 9.07% over twelve years. In contrast, the rate of FDG reduction in the control group was 2.2% over ten years. Based on these data, the researchers estimated that diminished FDG uptake started four and two years, respectively, before clinical indications of cognitive decline in subject A and B. These differences in time between glucose hypometabolism and onset of memory loss between subject A and B are probably due to heterogeneity in the characteristics of sporadic AD and inherited AD.

Lastly, several studies have reported the usefulness of heterogeneity in hypometabolism patterns in distinguishing different variants of AD [167–169]. Additionally, this heterogeneity turned out to be of value in predicting progression to different forms of dementia in the prodromal MCI phase [170].

### 3.2.3. Limitations

Although FDG-PET is thoroughly studied and seen as a robust biomarker of neurodegeneration [23], similar to other imaging techniques, FDG-PET has its limitations for the longitudinal monitoring of AD. Reduced glucose metabolism is not an AD-specific characteristic, but does also occur in a broad range of other diseases. For instance, FDG uptake is also diminished in certain brain regions after a stroke or other brain injuries [171]. Since approximately 30% of elderly people suffer from a silent infarct, lacking any clinical manifestations [172], alterations in cerebral glucose metabolism are not surprising in this aged population [173]. It is, therefore, suggested to consider FDG-PET as an independent biomarker rather than a biomarker of neurodegeneration in the "A/T/N" framework,

because, as mentioned before, FDG uptake is likely to reflect the glucose consumption by astrocytes instead of neurons [80,174]. In conclusion, FDG-PET is an effective technique in monitoring glucose metabolism in the brain, but it is a tool to measure glucose uptake rather than a biomarker for longitudinal monitoring of the neurodegenerative progression in AD.

### 3.3. Amyloid-PET

#### 3.3.1. Background

Although a fundamental role of A $\beta$  deposition in the pathogenesis of AD is widely accepted, the relationship between plaque density and disease severity is weak [175,176]. Multiple longitudinal studies have investigated the correlation in plaque density and cognitive decline.

#### 3.3.2. Findings

The goal of the study of Villemagne et al. was to visualize the longitudinal deposition of A $\beta$  and to investigate the relationship between A $\beta$  deposits and cognitive decline. Therefore, AD patients, MCI patients and age-matched healthy controls were recruited, and all subjects underwent PET imaging with PiB at baseline and follow-up. Low increased PiB retention at follow-up was found in AD and MCI patients, and in healthy controls with high retention at baseline. MCI subjects with high PiB retention had a higher chance to convert to AD than MCI patients with low PiB, and healthy controls with more PiB retention were at a higher risk to become MCI subjects than controls with low PiB. Although high levels of A $\beta$  accumulation predicted one's risk to convert to MCI or AD, the small increases in PiB retention only partly explained the cognitive decline, suggesting a more prominent role for other downstream factors. In a similar study by Koivonen et al., changes in A $\beta$  burden were evaluated over a period of two years [177]. In line with the previous described study, at baseline, MCI patients had higher PiB retention compared to controls. Additionally, uptake was elevated in MCI subjects that later converted to AD than non-converters, indicating that PiB retention time can predict conversion to AD. Another study consolidated the earlier findings by stating that a positive PiB scan is a strong indication for progression of MCI into AD [178]. Interestingly, during follow-up, the PiB uptake ratio increased in non-converters, while the retention time did not increase in converters, suggesting that PiB uptake only modestly changes once converted to AD. To further assess this assumption, longer follow-up time is needed.

Intensive longitudinal research in a group of two hundred participants revealed that A $\beta$  deposition progresses slowly, likely to be prolonged for more than twenty years [179]. Additionally, A $\beta$  seemed to slow down as the disease proceeded. Therefore, it is believed that as AD progresses, the A $\beta$  accumulation will reach a plateau (Figure 1), while the cognitive decline will intensify [86]. This finding was first reported by Jack et al. in a study that modelled the temporal trajectory of A $\beta$  deposition with PET imaging [180]. Over time, A $\beta$  deposition followed a sigmoidal-shaped trajectory, indicating that at high A $\beta$  load, an equilibrium is reached. In other words, A $\beta$  accumulation precedes cognitive decline, and once a quantitative plateau is reached, the disease will become more severe. This statement is further underlined by the hypothetical model of dynamic biomarkers [77,78]. Therefore, A $\beta$  accumulation may be a promising biomarker for predicting one's risk to convert from cognitively unimpaired to MCI or from MCI to AD (phase 1) but may be less useful as a marker to track disease progression once a patient has established AD (phase 2-5) (Figure 8). If A $\beta$  accumulation is no longer a dynamic marker of disease progression in the late stages of AD, it is assumed that other downstream factors are responsible for the observed associations between A $\beta$  deposition and altered brain structures [86].

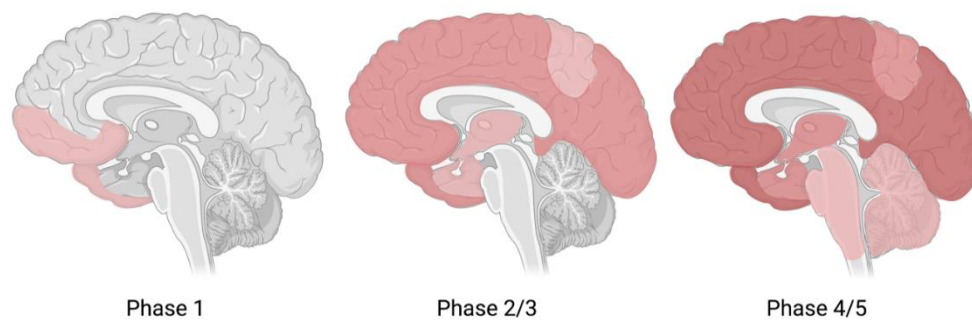


**Figure 8.** Spreading pattern of amyloid- $\beta$  accumulation throughout the brain. Amyloid- $\beta$  accumulation starts in frontal areas and spreads to other regions as disease progresses, leading to a plateau in amyloid- $\beta$  as disease progresses. Figure adapted from Goedert [145] and created with [www.BioRender.com](http://www.BioRender.com) (accessed on 11 February 2021).

### 3.3.3. Limitations

In addition to the limited value of A $\beta$  deposition in the longitudinal monitoring of already established AD, there are other limitations associated with A $\beta$  imaging for longitudinal monitoring of AD. For patients with already severe AD, it might be too difficult to lie still during the time needed to obtain the scans. Furthermore, PET imaging uses radiotracers, such as PiB and florbetapir. These radiotracers are known to target predominantly neuritic plaques [173]. Since these types of plaques are only scarcely presented in the cerebellum, this region is often used as a reference region for many A $\beta$ -PET studies [181]. However, multiple studies question the reliability of the cerebellum as a reference region for normalization in longitudinal A $\beta$  deposition, since it can affect the quantitative outcome in these longitudinal studies and lead to additional variability [182]. It has, therefore, been suggested to combine multiple reference regions into one more alike to the longitudinal changes to minimize potential variations [183].

## 3.4. Tau-PET

### 3.4.1. Background

As mentioned above, it is hypothesized that A $\beta$  burden reaches a plateau as AD progresses [180,184], making longitudinal tracking of A $\beta$  accumulation not the most promising biomarker for disease progression. On the other hand, tau levels slowly increase during the AD continuum with a steep increment approximately eight to nine years before disease onset (Figure 1) [21]. Therefore, longitudinal monitoring of tau accumulation may be a more powerful tool in monitoring disease progression. Moreover, increasing evidence suggests a close relationship between cognitive decline and tauopathy, making tau an interesting target for longitudinal monitoring of AD [185]. Since only recently the focus of research has shifted from A $\beta$  deposition modifying therapies to tau associated treatment, longitudinal research with tau-PET is still in the early stages compared to decades-long studies into A $\beta$  burden.

### 3.4.2. Findings

In 2015, Ishiki et al. performed a longitudinal study into tauopathy with the then novel radiotracer  $^{18}\text{F}$ -THK-5117 [186].  $^{18}\text{F}$ -THK5117 was significantly increased in middle and temporal gyri as well in the fusiform gyrus of AD patients. Higher levels of tau load were found in patients with more severe AD compared patients with mild AD. Additionally, these tauopathies were more widely spread across the cortical regions. Furthermore, uptake of  $^{18}\text{F}$ -THK5117 was strongly associated with the rate of cognitive decline, indicating a strong relationship between neurofibrillary pathology and neurodegenerative decline. This relationship may be useful in the longitudinal assessment of disease progression and the efficacy of therapies. The assumption is underlined by a large study investigating the relationship between tau accumulation, A $\beta$  deposition and cognitive impairment. The study included cognitively unimpaired subjects with normal A $\beta$  levels, subjects with no

cognitive impairment, but abnormal A $\beta$ , and cognitively impaired subjects with abnormal A $\beta$  and an amnesic phenotype [187]. The cognitively unimpaired group with normal A $\beta$  had no detectable tau accumulation throughout the brain, whereas the unimpaired abnormal A $\beta$  subjects had low, but significant rates (0.5% per year) of accumulation in multiple regions of the brain. This is in contrast to a study by Harrison et al. in which healthy adults with normal A $\beta$  showed observable tau accumulation associated with brain atrophy [188]. This might be due to the different radiotracers used in the studies. The cognitively impaired abnormal A $\beta$  subjects exhibited an increment in tau of 3% per year [187]. The accumulation rates differed only slightly from each other and during disease progression, accumulation rates increased consistently throughout the different brain areas. This indicated that tau accumulation is not restricted to one region at a time. Furthermore, the early increment in tau was not limited to the ERC, but rather widespread. Altogether, the study found that disease progression can be measured by increasing tau burden, and, therefore, tau accumulation rates may be useful as a clinical outcome for disease-modifying therapies.

The spreading of tau throughout the brain was further studied by Cho et al. in a research study into longitudinal changes in tau accumulation in cortical regions. In contrast to Jack et al., this study reported hierarchical spreading of tau from the entorhinal cortex to other brain regions (Figure 2) [189]. This typical topography of tau accumulation is believed to initiate in the ERC and with further neuronal degeneration and more cognitive decline, it spreads to other brain areas, such as the limbic regions and association cortices [4]. Moreover, tau accumulation rates in the ERC decrease as AD progresses to higher Braak stages.

Sintini et al. addressed the relationship between tau-PET uptake and brain atrophy in atypical AD. Interestingly, the regional patterns of tau accumulation and atrophy differed from one another in atypical AD [126]. High levels of tau accumulation were found in the frontal lobe, whereas atrophy rates were the greatest in temporoparietal areas. This difference suggested a temporal lag between tau deposition and the progression of neurodegeneration. This assumption has been previously proposed by other studies as well [114,115]. Furthermore, the research found that age has a negative effect on disease progression, since younger patients had higher rates of tau accumulation and atrophy. Lastly, there was a close relationship found between tau-PET uptake and gray matter volume.

### 3.4.3. Limitations

While tau accumulation is probably the most promising biomarker for disease progression, the heterogeneity of tau topography between the different AD subtypes is currently its major disadvantage [169,190]. Whereas amyloid distribution is believed to be similar, tau distribution varies between AD subtypes [59,125,191]. Additionally, each AD phenotype expresses a unique longitudinal regional pattern, and this pattern differs across the AD phenotypes [59]. It is, therefore, necessary to intensively study the dynamic patterns of AD biomarkers in atypical forms of AD in order to understand disease progression in these forms [169]. With extensive research into the different spreading patterns across the dementia spectrum, this disadvantage can become an advantage, as heterogeneity contributes to accurate longitudinal monitoring of the different AD types [190,192].

### 3.5. Summary

Over the years, great progress has been made in identifying biomarkers that reflect the disease progression of AD (Table 1). However, the distinct phenotypes of AD with corresponding heterogeneity in topographic patterns pose a challenge in the longitudinal monitoring of AD. Comprehensive research into the different subtypes of AD is needed to recognize these different patterns, and after correct identification, these pattern differences can be of additional value, such as for heterogeneity in hypometabolism patterns. Subsequently, clinical endpoints for disease-modifying therapies can be identified.

#### 4. Novel Methods, Applications of Imaging Techniques and Biomarkers in AD Research

Since there is still no effective treatment for AD and no perfect biomarker to detect AD from the earliest stages up to severe disease manifestation, much effort is put into finding novel techniques, new biomarkers and the development of new methods to apply existing techniques in the early diagnosis and longitudinal monitoring of AD. In this section, we briefly discuss new processing methods for existing techniques, possible new biomarkers that can contribute to monitoring AD and novel applications of imaging techniques in the search to successfully diagnose and monitor AD (Table 2).

**Table 2.** Summary of novel strategies in AD research.

<b>Methodology</b>	Voxel-based morphometry	Automated segmentation of brain tissues Comparison of voxels to measure concentration differences
	Deformation-based morphometry	Transformation of all brain volumes to standard template brain Statistical analysis of deformation fields
	Tensor-based morphometry	Uses regional differences in gradients of deformation Favored in large-scale MRI studies
	Pattern-based morphometry	Able to extract multidimensional characteristics More research necessary for broad application
	Data-driven methods	Large amounts of data can improve image quality More comparison between conventional and data-driven methods necessary
<b>Imaging technique</b>	Diffusion tensor imaging	Measures displacement of water in three dimensions Needs more research to exploit full potential
	Functional MRI	Uses BOLD signal for synaptic activity of neurons Not widely supported due to several limitations
	Optical coherence tomography	Non-invasive and cheap technique to assess effect of AD in the eye Reliability still question of debate
<b>Biomarker</b>	SV2A	Reflects synaptic density in brain Large scale validation necessary for broad application
	RAGE	Believed to regulate toxicity of A $\beta$ Potentially powerful biomarker in early diagnosis
	Iron	Relationship between A $\beta$ and iron accumulation Detection of iron with QSM promising tool

SV2A: synaptic glycoprotein 2A; RAGE: receptor for advanced glycation end products; QSM: quantitative susceptibility mapping.

##### 4.1. New Processing Methodologies for Existing Techniques

One way to increase the clinical value of already existing techniques is to improve the methods that process the obtained data. In the field of neuroimaging with MRI, much more clinical value has been obtained by using different morphometry methods for data processing. Since neuroimaging data of MRI scans are generally stored as matrices of voxels, there are several methodologies to process this type of data. Additionally, a high focus has been put on establishing new data-driven methods for the processing of PET images.

###### 4.1.1. Voxel-Based Morphometry

The most commonly used data-driven method for T1-weighted MRI images is voxel-based morphometry (VBM), which automatically segmentizes brain tissue in white matter, gray matter and CSF [193]. It transforms T1-weighted individual brain scans into a standard reference template. Subsequently, VBM measures differences in concentrations of the different brain tissues by comparing voxels of multiple brain regions [194]. In AD, VBM is used to quantify atrophy and to automatically distinguish AD patients from MCI subjects and healthy controls [195].

#### 4.1.2. Deformation-Based Morphometry

Another, more biologically related method, which was previously mentioned, is DBM, in which all brain volumes are transformed into a standard template brain [36,196]. In contrast to VBM, with DBM, the high resolution of the MRI images is maintained [36]. Instead of the voxels, the deformation fields that contain information about the spatial differences of the voxels between the imaged brain and the template brain are used for statistical analysis. Therefore, DBM is more sensitive for subtle changes in brain tissue composition than VBM. Additionally, data from multiple studies, imaging equipment and research centers can be processed without bias [197].

#### 4.1.3. Tensor-Based Morphometry

With tensor-based morphometry (TBM), regional differences in gradients of the deformation fields that line up the images into the template brain are measured [198]. TBM can be used in a wide range of assessments, varying from the voxel level to analysis of the whole brain. Moreover, since TBM is an almost fully automated process, it is favored in large-scale MRI studies, such as clinical trials.

#### 4.1.4. Pattern-Based Morphometry

Another type of morphometry is pattern-based morphometry (PBM), a method with its origin in VBM and DBM [199]. This data-driven method uses an algorithm based on sparse dictionary learning and is, in contrast to VBM, able to extract multidimensional patterns that characterize differences between groups, making PBM an interesting tool to compare different brain regions. Although PBM seems promising as a processing method for heterogenous disease, more research into robustness and extension to other types of neuroimaging is necessary for broad application.

#### 4.1.5. Data-Driven Methods

As technology improves, lately, much attention has been given to using large amounts of data to build data-driven models to improve the analysis of PET images. The effect of age on certain brain regions assessed with FDG-PET, for example, has been corrected using a data-driven approach [200]. Moreover, data-driven analysis of tau PET images identified spatial patterns of radiotracer  $^{18}\text{F}$ -AV1451 signal clusters compared to pathology-based methods, suggesting an advantage for data-driven methods in evaluating radiotracer data [201]. To fully benefit from the advantages of data-driven methods in neuroimaging, extra studies comparing conventional methods with data-driven methods are necessary.

### 4.2. Novel Implications of Imaging Techniques

In addition to new methodologies to increase the diagnostic value of already utilized imaging techniques, novel applications of other imaging techniques are increasing. Although structural MRI with T1-weighted images is still the gold standard in AD research with MRI, other MRI sequences seem to be promising.

#### 4.2.1. Diffusion Tensor Imaging

Diffusion tensor imaging (DTI) is an advanced type of diffusion MRI. This technique measures the displacement of water molecules in three dimensions to determine the integrity of the biological tissue [202,203]. In AD, DTI has been used to measure the integrity of brain regions by calculating the mean diffusivity [204]. Additionally, DTI demonstrated to be of value in determining the architecture of white matter [33], and multiple studies have reported the relationship between white matter integrity and disease severity, suggesting the inclusion of white matter degeneration as a pathological biomarker of AD for early diagnosis [205–207]. In order to exploit the full potential of DTI as a diagnostic tool in AD, the exact relationship between disease severity and white fiber tracts has to be explored [203].

#### 4.2.2. Functional MRI

Functional MRI (fMRI) is an imaging technique that gives insight into the functional integrity of brain networks that support several cognitive domains in a non-invasive manner [23,208]. fMRI uses the blood-oxygen-level-dependent (BOLD) signal to measure the synaptic activity of neurons. fMRI can be used in two manners: resting state (rs) fMRI, which measures changes in BOLD signals during inactivity, or task-related fMRI in which patients perform several cognitive tasks [33]. Since severely impaired patients may be too limited to perform these tasks, rsfMRI may be more feasible to monitor disease progression in later stages [23]. Although fMRI has been demonstrated to be of clinical value in studying the default mode network [209–212], clinical use of fMRI is not widely supported due to limitations, such as low signal and noise [202].

#### 4.2.3. Optical Coherence Tomography

Another interesting imaging technique to be applied in AD research is optical coherence tomography (OCT), but to date, there is no consensus on the employment of this technique. In recent years, pathological changes in the retina have been linked to AD [213]. These changes include A $\beta$  plaques, thinning of the retinal nerve fiber layer (RNFL), ganglion cell loss and decreased vessel density. Since OCT is a non-invasive, fast and inexpensive technique [214], multiple studies have investigated the beneficial value of OCT in AD research. Although accumulation of A $\beta$  in the lens, analysis of RNFL thickness and ganglion cell loss are proposed as diagnostic tools for AD [215–218], the reliability of these markers is still questioned due to possible other underlying diseases that cause these pathological changes, such as glaucoma. Nevertheless, the feasibility and cost effectiveness of OCT make it an interesting imaging technique to further investigate for applications in AD.

### 4.3. New Biomarkers

For many years, the focus of AD research has been on atrophy, glucose metabolism and imaging of A $\beta$  deposition and tau burden. However, since none of these biomarkers stands out as a faultless biomarker for the diagnosis of AD and disease progression, research focuses on identifying novel biomarkers that reflect the progression of AD. Over the years, several new biomarkers have been introduced.

#### 4.3.1. Synaptic Vesicle Glycoprotein 2A

One marker suggested to be of clinical value in AD is synaptic vesicle glycoprotein 2A (SV2A), which reflects the synaptic density [111]. This protein is located in the cell membrane of secretory vesicles, and since SV2A is ubiquitously expressed throughout the brain, lower levels of SV2A may be a promising biomarker of synaptic loss in AD. <sup>18</sup>F-UCB-J is a PET radiotracer considered to be sensitive for synaptic loss, because altered uptake of <sup>18</sup>F-UCB-J in the gray matter was correlated to altered expression of SV2A and lower synaptic density [219,220]. Although these results seem promising, large scale validation of this and other radiotracers is necessary to further exploit the clinical possibilities of SV2A in AD [9].

#### 4.3.2. Receptor for Advanced Glycation End Products

There is increasing evidence that the receptor for advanced glycation end products (RAGE) regulates the neurotoxicity of A $\beta$  in AD [221]. The binding of RAGE to A $\beta$  results in the release of reactive oxygen species that contribute to the formation of senile plaques and NFTs. Moreover, RAGE levels are significantly higher in AD subjects than in cognitively healthy controls [222]. Therefore, it has been suggested that in the early stages of AD, RAGE is a potent biomarker. <sup>11</sup>C-FPS-ZM1 is a radiotracer for PET imaging of RAGE in the brain [223]. Since RAGE overexpression is believed to precede the formation of A $\beta$  plaques, PET imaging of RAGE with <sup>11</sup>C-FPS-ZM1 may be a powerful tool in the early diagnosis of AD [221].

#### 4.3.3. Iron

Excessive accumulation of iron in specific brain parts is increasingly related to AD [224]. Although iron is required for maintaining homeostasis and plays a key role in many biological processes, abnormal accumulation of iron in subcortical and deep gray matter nuclei has been associated with AD [225]. Multiple studies have used quantitative susceptibility mapping (QSM) to quantify the local magnetic susceptibility derived from MRI images caused by deposits containing both A $\beta$  and iron [224,226,227]. QSM application in the detection of iron has been demonstrated to be of clinical value in assessing the relationship between A $\beta$  accumulation and iron burden [226]. Therefore, the detection of iron with QSM may be of potential aid in imaging A $\beta$  in the early diagnosis of AD [227].

### 5. Conclusions and Future Perspectives

In this review, we focused on the applications of imaging techniques in the early diagnosis and longitudinal monitoring of AD. AD is a neurodegenerative disease in which pathological changes occur decades before disease manifestation. The disease is characterized by the formation of senile plaques, NFTs and subsequent synaptic loss and neurodegeneration. Although AD affects a major part of the population worldwide, to date, there is no therapy to cure AD. Since disease-modifying therapies may be the most beneficial in early stages of the disease, it is important to diagnose AD as early as possible. Additionally, longitudinal monitoring of disease progression is crucial to gain a better understanding of the pathogenesis and to set clinical endpoints for potential treatment. To date, several biomarkers have been proposed for the early diagnosis and longitudinal monitoring of AD, but all these biomarkers have their limitations regarding specificity, reliability and sensitivity.

A $\beta$  deposition is among the earliest hallmarks of AD, but to date, there is no consensus on exactly how A $\beta$  accumulation contributes to the pathogenesis of AD. Moreover, detailed study into A $\beta$  over time has revealed that A $\beta$  levels reach an equilibrium, making A $\beta$  a questionable biomarker for monitoring disease progression. Tau accumulation, on the other hand, is believed to be more biologically related to the symptoms associated with neurodegeneration in AD. Imaging studies with tau PET-tracers have demonstrated promising results, but compared to A $\beta$ -PET imaging, large-scale validation of these tracers must be performed to make tau-PET imaging a reliable tool in AD. Moreover, longitudinal studies into different phenotypes of AD revealed heterogeneity in the topographic patterns of tau accumulation throughout the brain. This heterogeneity can be of additional value, but first, more detailed study in these different tau spreading patterns is required. More general imaging techniques, such as FDG-PET and structural MRI, have been applied in AD research, but these techniques measure rather more common pathological changes than AD-specific characteristics. Brain atrophy, measured by structural MRI, is not restricted to AD pathology and is only detectable after a substantial amount of neurodegeneration. FDG-PET is used to measure the glucose uptake in the brain. Since synaptic loss in AD leads to hypometabolism, decreased glucose uptake is associated with AD. However, decreased glucose metabolism is not restricted to AD but can also occur after strokes and brain injury. Furthermore, an increasing body of evidence suggests that glucose uptake reflects astrocyte function rather than neuronal function.

Altogether, to date, there is no perfect biomarker to detect AD in the early stages and to monitor disease progression over time. Furthermore, these biomarkers rely on neuroimaging techniques that require high-quality and expensive machinery, making them infeasible for large-scale examinations of greater populations.

Hence, comprehensive and in-depth research into AD is crucial in the early diagnosis and longitudinal monitoring of AD. Since tau-PET appears to be the most promising tool for the diagnosis and tracking of disease progression, the field of research should focus on the validation and development of existing and new tau radiotracers. Furthermore, detailed research into new applications of other imaging techniques is necessary to overcome the limitations in the extensive scanning of large populations. Lastly, current tools require

relatively high levels of protein accumulation or neurodegeneration to be detectable. Since higher levels are associated with higher disease severity and lower beneficial potential of therapies, identifying novel biomarkers that reflect the pathogenesis of AD in the earliest stages is essential for the development of disease-modifying therapies.

**Author Contributions:** W.M.v.O., writing—original draft preparation; E.C.M.d.L., writing—review and editing; E.C.M.d.L., supervision. All authors have read and agreed to the published version of the manuscript.

**Funding:** This research received no external funding.

**Institutional Review Board Statement:** Not applicable.

**Informed Consent Statement:** Not applicable.

**Conflicts of Interest:** The authors declare no conflict of interest.

## Abbreviations

AD	Alzheimer's disease
NFT	Neurofibrillary tangle
A $\beta$	Amyloid- $\beta$
MRI	Magnetic resonance imaging
PET	Positron emission tomography
MCI	Mild cognitive impairment
CNS	Central nervous system
FDG-PET	Fluorodeoxyglucose positron emission tomography
APP	Amyloid precursor protein
CSF	Cerebrospinal fluid
PiB	Pittsburgh compound-B
FTD	Frontotemporal dementia
PHF	Paired helical fragment
BBB	Blood-brain barrier
MMSE	Mini-mental state examination
DBM	Deformation-based morphometry
ERC	Entorhinal cortex
MTA	Medial temporal lobe atrophy
aMCI	Amnesic mild cognitive impairment
ADNI	Alzheimer's Disease Neuroimaging Initiative
VBM	Voxel-based morphometry
TBM	Tensor-based morphometry
fMRI	Functional magnetic resonance imaging
BOLD	Blood-oxygen-level-dependent
rsfMRI	Resting state functional magnetic resonance imaging
DTI	Diffusion tensor imaging
OCT	Optical coherence tomography
RNFL	Retinal nerve fiber layer
SV2A	Synaptic vesicle glycoprotein 2A
RAGE	Receptor for advanced glycation end products
QSM	Quantitative susceptibility mapping

## References

- Henry, M.S.; Passmore, A.P.; Todd, S.; McGuinness, B.; Craig, D.; Johnston, J.A. The development of effective biomarkers for Alzheimer's disease: A review. *Int. J. Geriatr. Psychiatry* **2013**, *28*, 331–340. [[CrossRef](#)] [[PubMed](#)]
- Lynch, C. World Alzheimer Report 2019: Attitudes to dementia, a global survey. *Alzheimer's Dement.* **2020**, *16*, e038255. [[CrossRef](#)]
- Braak, H.; Braak, E. Neuropathological staging of Alzheimer-related changes. *Acta Neuropathol.* **1991**, *82*, 239–259. [[CrossRef](#)] [[PubMed](#)]
- Valotassiou, V.; Malamitsi, J.; Papatriantafyllou, J.; Dardiotis, E.; Tsougos, I.; Psimadas, D.; Alexiou, S.; Hadjigeorgiou, G.; Georgoulas, P. SPECT and PET imaging in Alzheimer's disease. *Ann. Nucl. Med.* **2018**, *32*, 583–593. [[CrossRef](#)] [[PubMed](#)]

5. Cras, P.; Kawai, M.; Lowery, D.; Gonzalez-DeWhitt, P.; Greenberg, B.; Perry, G. Senile plaque neurites in Alzheimer disease accumulate amyloid precursor protein. *Proc. Natl. Acad. Sci. USA* **1991**, *88*, 7552–7556. [[CrossRef](#)]
6. Gong, N.J.; Chan, C.C.; Leung, L.M.; Wong, C.S.; Dibb, R.; Liu, C. Differential microstructural and morphological abnormalities in mild cognitive impairment and Alzheimer's disease: Evidence from cortical and deep gray matter. *Hum. Brain Mapp.* **2017**, *38*, 2495–2508. [[CrossRef](#)]
7. Okamura, N.; Harada, R.; Ishiki, A.; Kikuchi, A.; Nakamura, T.; Kudo, Y. The development and validation of tau PET tracers: Current status and future directions. *Clin. Transl. Imaging* **2018**, *6*, 305–316. [[CrossRef](#)] [[PubMed](#)]
8. Querfurth, H.W.; LaFerla, F.M. Alzheimer's Disease. *N. Engl. J. Med.* **2010**, *362*, 329–344. [[CrossRef](#)] [[PubMed](#)]
9. Cai, Z.; Li, S.; Matuskey, D.; Nabulsi, N.; Huang, Y. PET imaging of synaptic density: A new tool for investigation of neuropsychiatric diseases. *Neurosci. Lett.* **2019**, *691*, 44–50. [[CrossRef](#)] [[PubMed](#)]
10. Wisniewski, T.; Drummond, E. Future horizons in Alzheimer's disease research. *Prog. Mol. Biol. Transl. Sci.* **2019**, *168*, 223–241. [[CrossRef](#)]
11. Tiwari, S.; Atluri, V.; Kaushik, A.; Yndart, A.; Nair, M. Alzheimer's disease: Pathogenesis, diagnostics, and therapeutics. *Int. J. Nanomed.* **2019**, *14*, 5541–5554. [[CrossRef](#)]
12. Blennow, K.; de Leon, M.J.; Zetterberg, H. Alzheimer's disease. *Lancet* **2006**, *368*, 387–403. [[CrossRef](#)]
13. Dubois, B.; Hampel, H.; Feldman, H.H.; Scheltens, P.; Aisen, P.; Andrieu, S.; Bakardjian, H.; Benali, H.; Bertram, L.; Blennow, K.; et al. Preclinical Alzheimer's disease: Definition, natural history, and diagnostic criteria. *Alzheimers. Dement.* **2016**, *12*, 292–323. [[CrossRef](#)] [[PubMed](#)]
14. Lawrence, E.; Vegvari, C.; Ower, A.; Hadjichrysanthou, C.; De Wolf, F.; Anderson, R.M. A systematic review of longitudinal studies which measure Alzheimer's disease biomarkers. *J. Alzheimer's Dis.* **2017**, *59*, 1359–1379. [[CrossRef](#)]
15. Hampel, H.; Shen, Y.; Walsh, D.M.; Aisen, P.; Shaw, L.M.; Zetterberg, H.; Trojanowski, J.Q.; Blennow, K. Biological markers of amyloid  $\beta$ -related mechanisms in Alzheimer's disease. *Exp. Neurol.* **2010**, *223*, 334–346. [[CrossRef](#)] [[PubMed](#)]
16. Mosconi, L. Glucose metabolism in normal aging and Alzheimer's disease: Methodological and physiological considerations for PET studies. *Clin. Transl. Imaging* **2013**, *1*, 217–233. [[CrossRef](#)]
17. Jack, C.R.; Albert, M.; Knopman, D.S.; Mckhann, G.M.; Sperling, R.A.; Carillo, M.; Thies, W.; Phelps, C.H. Introduction to revised criteria for the diagnosis of Alzheimer's disease: National Institute on Aging and the Alzheimer Association Workgroups. *Alzheimer Dement.* **2011**, *7*, 257–262. [[CrossRef](#)] [[PubMed](#)]
18. Jack, C.R.; Bennett, D.A.; Blennow, K.; Carrillo, M.C.; Feldman, H.H.; Frisoni, G.B.; Hampel, H.; Jagust, W.J.; Johnson, K.A.; Knopman, D.S.; et al. A/T/N: An unbiased descriptive classification scheme for Alzheimer disease biomarkers. *Neurology* **2016**, *87*, 539–547. [[CrossRef](#)] [[PubMed](#)]
19. Jack, C.R.; Bennett, D.A.; Blennow, K.; Carrillo, M.C.; Dunn, B.; Haeblerlein, S.B.; Holtzman, D.M.; Jagust, W.; Jessen, F.; Karlawish, J.; et al. NIA-AA Research Framework: Toward a biological definition of Alzheimer's disease. *Alzheimer's Dement.* **2018**, *14*, 535–562. [[CrossRef](#)]
20. Counts, S.E.; Ikonovic, M.D.; Mercado, N.; Vega, I.E.; Mufson, E.J. Biomarkers for the Early Detection and Progression of Alzheimer's Disease. *Neurotherapeutics* **2017**, *14*, 35–53. [[CrossRef](#)] [[PubMed](#)]
21. Yoshiyama, Y.; Lee, V.M.Y.; Trojanowski, J.Q. Therapeutic strategies for tau mediated neurodegeneration. *J. Neurol. Neurosurg. Psychiatry* **2013**, *84*, 784–795. [[CrossRef](#)]
22. Chun, K.A. Beta-amyloid imaging in dementia. *Yeungnam Univ. J. Med.* **2018**, *35*, 1–6. [[CrossRef](#)]
23. Johnson, K.A.; Fox, N.C.; Sperling, R.A.; Klunk, W.E.; Queiroz, L.; Nucci, A.; Fature, N.O.; Fature, J.J.; Johnson, K.A.; Fox, N.C.; et al. Brain imaging in Alzheimer disease. *Cold Spring Harb. Perspect. Med.* **2012**, *2*, a006213. [[CrossRef](#)]
24. Liu, X.; Chen, K.; Wu, T.; Weidman, D.; Lure, F.; Li, J. Use of multimodality imaging and artificial intelligence for diagnosis and prognosis of early stages of Alzheimer's disease. *Transl. Res.* **2018**, *194*, 56–67. [[CrossRef](#)] [[PubMed](#)]
25. Jack, C.R.; Dickson, D.W.; Parisi, J.E.; Xu, Y.C.; Cha, R.H.; O'Brien, P.C.; Edland, S.D.; Smith, G.E.; Boeve, B.F.; Tangalos, E.G.; et al. Antemortem MRI findings correlate with hippocampal neuropathology in typical aging and dementia. *Neurology* **2002**, *58*, 750–757. [[CrossRef](#)]
26. De Leon, M.J.; Desanti, S.; Zinkowski, R.; Mehta, P.D.; Pratico, D.; Segal, S.; Clark, C.; Kerkman, D.; Debernardis, J.; Li, J.; et al. MRI and CSF studies in the early diagnosis of Alzheimer's disease. *J. Intern. Med.* **2004**, *256*, 205–223. [[CrossRef](#)] [[PubMed](#)]
27. Colliot, O.; Chételat, G.; Chupin, M.; Desgranges, B.; Magnin, B.; Benali, H.; Dubois, B.; Garnero, L.; Eustache, F.; Lehericy, S. Discrimination between Alzheimer Disease, Mild Cognitive Impairment, and Normal Aging by Using Automated Segmentation of the Hippocampus. *Radiology* **2008**, *248*, 194–201. [[CrossRef](#)] [[PubMed](#)]
28. Bobinski, M.; De Leon, M.J.; Wegiel, J.; Desanti, S.; Convit, A.; Saint Louis, L.A.; Rusinek, H.; Wisniewski, H.M. The histological validation of post mortem magnetic resonance imaging-determined hippocampal volume in Alzheimer's disease. *Neuroscience* **1999**, *95*, 721–725. [[CrossRef](#)]
29. Du, A.T.; Schuff, N.; Amend, D.; Laakso, M.P.; Hsu, Y.Y.; Jagust, W.J.; Yaffe, K.; Kramer, J.H.; Reed, B.; Norman, D.; et al. Magnetic resonance imaging of the entorhinal cortex and hippocampus in mild cognitive impairment and Alzheimer's disease. *J. Neurol. Neurosurg. Psychiatry* **2001**, *71*, 441–447. [[CrossRef](#)]
30. Waser, M.; Benke, T.; Dal-Bianco, P.; Garn, H.; Mosbacher, J.A.; Ransmayr, G.; Schmidt, R.; Seiler, S.; Sorensen, H.B.D.; Jennum, P.J. Neuroimaging markers of global cognition in early Alzheimer's disease: A magnetic resonance imaging–electroencephalography study. *Brain Behav.* **2019**, *9*, 1–11. [[CrossRef](#)] [[PubMed](#)]

31. Pennanen, C.; Kivipelto, M.; Tuomainen, S.; Hartikainen, P.; Hänninen, T.; Laakso, M.P.; Hallikainen, M.; Vanhanen, M.; Nissinen, A.; Helkala, E.-L.; et al. Hippocampus and entorhinal cortex in mild cognitive impairment and early AD. *Neurobiol. Aging* **2004**, *25*, 303–310. [[CrossRef](#)]
32. Killiany, R.J.; Hyman, B.T.; Gomez-Isla, T.; Moss, M.B.; Kikinis, R.; Jolesz, F.; Tanzi, R.; Jones, K.; Albert, M.S. MRI measures of entorhinal cortex vs hippocampus in preclinical AD. *Neurology* **2002**, *58*, 1188–1196. [[CrossRef](#)]
33. Teipel, S.J.; Grothe, M.; Lista, S.; Toschi, N.; Garaci, F.G.; Hampel, H. Relevance of Magnetic Resonance Imaging for Early Detection and Diagnosis of Alzheimer Disease. *Med. Clin. N. Am.* **2013**, *97*, 399–424. [[CrossRef](#)]
34. Xu, Y.; Jack, C.R.J.; O'Brien, P.C.; Kokmen, E.; Smith, G.E.; Ivnik, R.J.; Boeve, B.F.; Tangalos, R.G.; Petersen, R.C. Usefulness of MRI measures of entorhinal cortex versus hippocampus in AD. *Neurology* **2000**, *54*, 1760–1767. [[CrossRef](#)] [[PubMed](#)]
35. De Leon, M.J.; Bobinski, M.; Convit, A.; Wolf, O.; Insausti, R. Usefulness of MRI measures of entorhinal cortex versus hippocampus in AD. *Neurology* **2001**, *56*, 820–823. [[CrossRef](#)]
36. Hampel, H.; Bürger, K.; Teipel, S.J.; Bokde, A.L.W.; Zetterberg, H.; Blennow, K. Core candidate neurochemical and imaging biomarkers of Alzheimer's disease. *Alzheimer's Dement.* **2008**, *4*, 38–48. [[CrossRef](#)] [[PubMed](#)]
37. Lerch, J.P.; Pruessner, J.C.; Zijdenbos, A.; Hampel, H.; Teipel, S.J.; Evans, A.C. Focal decline of cortical thickness in Alzheimer's disease identified by computational neuroanatomy. *Cereb. Cortex* **2005**, *15*, 995–1001. [[CrossRef](#)]
38. Dickerson, B.C.; Bakkour, A.; Salat, D.H.; Feczko, E.; Pacheco, J.; Greve, D.N.; Grodstein, F.; Wright, C.I.; Blacker, D.; Rosas, H.D.; et al. The cortical signature of Alzheimer's disease: Regionally specific cortical thinning relates to symptom severity in very mild to mild AD dementia and is detectable in asymptomatic amyloid-positive individuals. *Cereb. Cortex* **2009**, *19*, 497–510. [[CrossRef](#)]
39. Dickerson, B.C.; Stoub, T.R.; Shah, R.C.; Sperling, R.A.; Killiany, R.J.; Albert, M.S.; Hyman, B.T.; Blacker, D.; Detolledo-Morrell, L. Alzheimer-signature MRI biomarker predicts AD dementia in cognitively normal adults. *Neurology* **2011**, *76*, 1395–1402. [[CrossRef](#)] [[PubMed](#)]
40. Im, K.; Lee, J.M.; Seo, S.W.; Yoon, U.; Kim, S.T.; Kim, Y.H.; Kim, S.I.; Na, D.L. Variations in cortical thickness with dementia severity in Alzheimer's disease. *Neurosci. Lett.* **2008**, *436*, 227–231. [[CrossRef](#)]
41. Busovaca, E.; Zimmerman, M.E.; Meier, I.B.; Griffith, E.Y.; Grieve, S.M.; Korgaonkar, M.S.; Williams, L.M.; Brickman, A.M. Is the Alzheimer's disease cortical thickness signature a biological marker for memory? *Brain Imaging Behav.* **2016**, *10*, 517–523. [[CrossRef](#)] [[PubMed](#)]
42. Ossenkoppele, R.; Smith, R.; Ohlsson, T.; Strandberg, O.; Mattsson, N.; Insel, P.S.; Palmqvist, S.; Hansson, O. Associations between tau, A $\beta$ , and cortical thickness with cognition in Alzheimer disease. *Neurology* **2019**, *92*, e601–e612. [[CrossRef](#)]
43. Henriques, A.D.; Benedet, A.L.; Camargos, E.F.; Rosa-Neto, P.; Nóbrega, O.T. Fluid and imaging biomarkers for Alzheimer's disease: Where we stand and where to head to. *Exp. Gerontol.* **2018**, *107*, 169–177. [[CrossRef](#)]
44. Frisoni, G.B.; Fox, N.C.; Jack, C.R.; Scheltens, P.; Thompson, P.M. The clinical use of structural MRI in Alzheimer disease. *Nat. Rev. Neurol.* **2010**, *6*, 67–77. [[CrossRef](#)]
45. Geuze, E.; Vermetten, E.; Bremner, J.D. MR-based in vivo hippocampal volumetrics: 2. Findings in neuropsychiatric disorders. *Mol. Psychiatry* **2005**, *10*, 160–184. [[CrossRef](#)]
46. Camicioli, R.; Moore, M.M.; Kinney, A.; Corbridge, E.; Glassberg, K.; Kaye, J.A. Parkinson's disease is associated with hippocampal atrophy. *Mov. Disord.* **2003**, *18*, 784–790. [[CrossRef](#)] [[PubMed](#)]
47. Allebone, J.; Kanaan, R.; Maller, J.; O'Brien, T.; Mullen, S.A.; Cook, M.; Adams, S.J.; Vogrin, S.; Vaughan, D.N.; Connelly, A.; et al. Bilateral volume reduction in posterior hippocampus in psychosis of epilepsy. *J. Neurol. Neurosurg. Psychiatry* **2019**, *90*, 688–694. [[CrossRef](#)]
48. Rosas, H.D.; Koroshetz, W.J.; Chen, Y.I.; Skeuse, C.; Vangel, M.; Cudkowicz, M.E.; Caplan, K.; Marek, K.; Seidman, L.J.; Makris, N.; et al. Evidence for more widespread cerebral pathology in early HD: An MRI-based morphometric analysis. *Neurology* **2003**, *60*, 1615–1620. [[CrossRef](#)] [[PubMed](#)]
49. Fujioka, M.; Nishio, K.; Miyamoto, S.; Hiramatsu, K.I.; Sakaki, T.; Okuchi, K.; Taoka, T.; Fujioka, S. Hippocampal damage in the human brain after cardiac arrest. *Cerebrovasc. Dis.* **2000**, *10*, 2–7. [[CrossRef](#)]
50. Agartz, I.; Momenan, R.; Rawlings, R.R.; Kerich, M.J.; Hommer, D.W. Hippocampal volume in patients with alcohol dependence. *Arch. Gen. Psychiatry* **1999**, *56*, 356–363. [[CrossRef](#)] [[PubMed](#)]
51. Abernethy, L.J.; Palaniappan, M.; Cooke, R.W.I. Quantitative magnetic resonance imaging of the brain in survivors of very low birth weight. *Arch. Dis. Child.* **2002**, *87*, 279–283. [[CrossRef](#)]
52. Lee, S.; Lee, H.; Kim, K.W. Magnetic resonance imaging texture predicts progression to dementia due to Alzheimer disease earlier than hippocampal volume. *J. Psychiatry Neurosci.* **2020**, *45*, 7–14. [[CrossRef](#)] [[PubMed](#)]
53. Macdonald, K.E.; Leung, K.K.; Bartlett, J.W.; Blair, M.; Malone, I.B.; Barnes, J.; Ourselin, S.; Fox, N.C. Automated template-based hippocampal segmentations from MRI: The effects of 1.5T or 3T field strength on accuracy. *Neuroinformatics* **2014**, *12*, 405–412. [[CrossRef](#)]
54. Cash, D.M.; Rohrer, J.D.; Ryan, N.S.; Ourselin, S.; Fox, N.C. Imaging endpoints for clinical trials in Alzheimer's disease. *Alzheimer's Res. Ther.* **2014**, *6*, 1–10. [[CrossRef](#)]
55. Chupin, M.; Gérardin, E.; Cuingnet, R.; Boutet, C.; Lemieux, L.; Lehericy, S.; Benali, H.; Garnero, L.; Colliot, O. Fully automatic hippocampus segmentation and classification in Alzheimer's disease and mild cognitive impairment applied on data from ADNI. *Hippocampus* **2009**, *19*, 579–587. [[CrossRef](#)]

56. Hurtz, S.; Chow, N.; Watson, A.E.; Somme, J.H.; Goukasian, N.; Hwang, K.S.; Morra, J.; Elashoff, D.; Gao, S.; Petersen, R.C.; et al. Automated and manual hippocampal segmentation techniques: Comparison of results, reproducibility and clinical applicability. *NeuroImage Clin.* **2019**, *21*. [[CrossRef](#)]
57. Xie, L.; Wisse, L.E.M.; Pluta, J.; de Flores, R.; Piskin, V.; Manjón, J.V.; Wang, H.; Das, S.R.; Ding, S.L.; Wolk, D.A.; et al. Automated segmentation of medial temporal lobe subregions on in vivo T1-weighted MRI in early stages of Alzheimer's disease. *Hum. Brain Mapp.* **2019**, *40*, 3431–3451. [[CrossRef](#)]
58. Firth, N.C.; Primativo, S.; Marinescu, R.V.; Shakespeare, T.J.; Suarez-Gonzalez, A.; Lehmann, M.; Carton, A.; Ocal, D.; Pavisic, I.; Paterson, R.W.; et al. Longitudinal neuroanatomical and cognitive progression of posterior cortical atrophy. *Brain* **2019**, *142*, 2082–2095. [[CrossRef](#)] [[PubMed](#)]
59. Sintini, I.; Graff-Radford, J.; Senjem, M.L.; Schwarz, C.G.; Machulda, M.M.; Martin, P.R.; Jones, D.T.; Boeve, B.F.; Knopman, D.S.; Kantarci, K.; et al. Longitudinal neuroimaging biomarkers differ across Alzheimer's disease phenotypes. *Brain* **2020**, *143*, 2281–2294. [[CrossRef](#)] [[PubMed](#)]
60. Panegyres, P.K.; Rogers, J.M.; McCarthy, M.; Campbell, A.; Wu, J.S. Fluorodeoxyglucose-positron emission tomography in the differential diagnosis of early-onset dementia: A prospective, community-based study. *BMC Neurol.* **2009**, *9*, 1–9. [[CrossRef](#)] [[PubMed](#)]
61. Hampel, H.; Frank, R.; Broich, K.; Teipel, S.J.; Katz, R.G.; Hardy, J.; Herholz, K.; Bokde, A.L.W.; Jessen, F.; Hoessler, Y.C.; et al. Biomarkers for alzheimer's disease: Academic, industry and regulatory perspectives. *Nat. Rev. Drug Discov.* **2010**, *9*, 560–574. [[CrossRef](#)]
62. Marcus, C.; Mena, E.; Subramaniam, R.M. Brain PET in the diagnosis of Alzheimer's disease. *Clin. Nucl. Med.* **2014**, *39*, e413–e426. [[CrossRef](#)] [[PubMed](#)]
63. Benson, D.F.; Kuhl, D.E.; Hawkins, R.A.; Phelps, M.E.; Cummings, J.L.; Tsai, S.Y. The Fluorodeoxyglucose 18F Scan in Alzheimer's Disease and Multi-infarct Dementia. *Arch. Neurol.* **1983**, *40*, 711–714. [[CrossRef](#)] [[PubMed](#)]
64. Friedland, R.P.; Budinger, T.F.; Ganz, E.; Yano, Y.; Mathis, C.A.; Koss, B.; Ober, B.A.; Huesman, R.H.; Derenzo, S.E. Regional cerebral metabolic alterations in dementia of the Alzheimer type: Positron emission tomography with [<sup>18</sup>F] fluorodeoxyglucose. *J. Comput. Assist. Tomogr.* **1983**, *7*, 590–598. [[CrossRef](#)]
65. Foster, N.L.; Chase, T.N.; Fedio, P.; Patronas, N.J.; Brooks, R.A.; Di Chiro, G. Alzheimer's disease: Focal cortical changes shown by positron emission tomography. *Neurology* **1983**, *33*, 961–965. [[CrossRef](#)] [[PubMed](#)]
66. McGeer, P.L.; Kamo, H.; Harrop, R.; Li, D.K.; Tuokko, H.; Adam, M.J.; Ammann, W.; Beattie, B.L.; Calne, D.B. Positron emission tomography in patients with clinically diagnosed Alzheimer's disease. *Can. Med. Assoc. J.* **1986**, *134*, 597–607.
67. Herholz, K. FDG PET and differential diagnosis of dementia. *Alzheimer Dis. Assoc. Disord.* **1995**, *9*, 6–16. [[CrossRef](#)]
68. Minoshima, S.; Frey, K.A.; Koeppe, R.A.; Foster, N.L.; Kuhl, D.E. A diagnostic approach in Alzheimer's disease using three-dimensional stereotactic surface projections of fluorine-18-FDG PET. *J. Nucl. Med.* **1995**, *36*, 1238–1248.
69. Silverman, D.H.S.; Small, G.W.; Chang, C.Y.; Lu, C.S.; de Aburto, M.A.K.; Chen, W.; Czernin, J.; Rapoport, S.I.; Pietrini, P.; Alexander, G.E.; et al. Positron Emission Tomography in Evaluation of Dementia Regional Brain Metabolism and Long-term Outcome. *JAMA* **2001**, *286*, 2120–2127. [[CrossRef](#)]
70. Hoffman, J.M.; Welsh-Bohmer, K.A.; Hanson, M.; Crain, B.; Hulette, C.; Earl, N.; Coleman, R.E. FDG PET imaging in patients with pathologically verified dementia. *J. Nucl. Med.* **2000**, *41*, 1920–1928. [[PubMed](#)]
71. Jagust, W.; Reed, B.; Mungas, D.; Ellis, W.; DeCarli, C. What does fluorodeoxyglucose PET imaging add to a clinical diagnosis of dementia? *Neurology* **2007**, *69*, 871–877. [[CrossRef](#)]
72. Bloudek, L.M.; Spackman, D.E.; Blankenburg, M.; Sullivan, S.D. Review and meta-analysis of biomarkers and diagnostic imaging in Alzheimer's disease. *J. Alzheimer's Dis.* **2011**, *26*, 627–645. [[CrossRef](#)]
73. Patwardhan, M.B.; McCrory, D.C.; Matchar, D.B.; Samsa, G.P.; Rutschmann, O.T. Alzheimer Disease: Operating Characteristics of PET—A Meta-Analysis. *Radiology* **2004**, *231*, 73–80. [[CrossRef](#)] [[PubMed](#)]
74. Bohnen, N.I.; Djang, D.S.W.; Herholz, K.; Anzai, Y.; Minoshima, S. Effectiveness and safety of 18F-FDG PET in the evaluation of dementia: A review of the recent literature. *J. Nucl. Med.* **2012**, *53*, 59–71. [[CrossRef](#)]
75. Mosconi, L.; Berti, V.; Glodzik, L.; Pupi, A.; De Santi, S.; de Leon, M.J. Pre-clinical detection of Alzheimer's disease using FDG-PET, with or without amyloid imaging. *J. Alzheimers. Dis.* **2010**, *20*, 843–854. [[CrossRef](#)] [[PubMed](#)]
76. De Santi, S.; De Leon, M.J.; Rusinek, H.; Convit, A.; Tarshish, C.Y.; Roche, A.; Tsui, W.H.; Kandil, E.; Boppana, M.; Daisley, K.; et al. Hippocampal formation glucose metabolism and volume losses in MCI and AD. *Neurobiol. Aging* **2001**, *22*, 529–539. [[CrossRef](#)]
77. Jack, C.R.; Knopman, D.S.; Jagust, W.J.; Petersen, R.C.; Weiner, M.W.; Aisen, P.S.; Shaw, L.M.; Vemuri, P.; Wiste, H.J.; Weigand, S.D.; et al. Tracking pathophysiological processes in Alzheimer's disease: An updated hypothetical model of dynamic biomarkers. *Lancet Neurol.* **2013**, *12*, 207–216. [[CrossRef](#)]
78. Jack, C.R.; Knopman, D.S.; Jagust, W.J.; Shaw, L.M.; Aisen, P.S.; Weiner, M.W.; Petersen, R.C.; Trojanowski, J.Q. Hypothetical model of dynamic biomarkers of the Alzheimer's pathological cascade. *Lancet Neurol.* **2010**, *9*, 119–128. [[CrossRef](#)]
79. Drzezga, A.; Altomare, D.; Festari, C.; Arbizu, J.; Orini, S.; Herholz, K.; Nestor, P.; Agosta, F.; Bouwman, F.; Nobili, F.; et al. Diagnostic utility of 18F-Fluorodeoxyglucose positron emission tomography (FDG-PET) in asymptomatic subjects at increased risk for Alzheimer's disease. *Eur. J. Nucl. Med. Mol. Imaging* **2018**, *45*, 1487–1496. [[CrossRef](#)]

80. Zimmer, E.R.; Parent, M.J.; Souza, D.G.; Leuzy, A.; Lecrux, C.; Kim, H.I.; Gauthier, S.; Pellerin, L.; Hamel, E.; Rosa-Neto, P. [18F]FDG PET signal is driven by astroglial glutamate transport. *Nat. Neurosci.* **2017**, *20*, 393–395. [[CrossRef](#)]
81. Vanhoutte, M.; Lopes, R.; Maureille, A.; Delmaire, C.; Hossein-Foucher, C.; Rollin, A.; Semah, F.; Pasquier, F. P1-291: Hypometabolism Patterns Using FDG-PET in Typical and Atypical Sporadic Forms of Early-Onset Alzheimer's Disease. *Alzheimer's Dement.* **2016**, *12*, P532. [[CrossRef](#)]
82. Hardy, J.; Higgins, G. Alzheimer's disease: The amyloid cascade hypothesis. *Science* **1992**, *256*, 184–185. [[CrossRef](#)]
83. Hardy, J.; Selkoe, D. The amyloid hypothesis of Alzheimer's disease: Progress and problems on the road to therapeutics. *Science* **2002**, *297*, 353–356. [[CrossRef](#)] [[PubMed](#)]
84. Morris, G.P.; Clark, I.A.; Vissel, B. Questions concerning the role of amyloid- $\beta$  in the definition, aetiology and diagnosis of Alzheimer's disease. *Acta Neuropathol.* **2018**, *136*, 663–689. [[CrossRef](#)]
85. Swerdlow, R.H. Alzheimer's disease pathologic cascades: Who comes first, what drives what. *Neurotox. Res.* **2012**, *22*, 182–194. [[CrossRef](#)]
86. Meyer, P.F.; McSweeney, M.; Gonneaud, J.; Villeneuve, S. AD molecular: PET amyloid imaging across the Alzheimer's disease spectrum: From disease mechanisms to prevention. *Prog. Mol. Biol. Transl. Sci.* **2019**, *165*, 63–106. [[CrossRef](#)] [[PubMed](#)]
87. Ono, K. Alzheimer's disease as oligomeropathy. *Neurochem. Int.* **2018**, *119*, 57–70. [[CrossRef](#)] [[PubMed](#)]
88. Selkoe, D.J.; Hardy, J. The amyloid hypothesis of Alzheimer's disease at 25 years. *EMBO Mol. Med.* **2016**, *8*, 595–608. [[CrossRef](#)] [[PubMed](#)]
89. Patterson, C.; Feightner, J.W.; Garcia, A.; Hsiung, G.-Y.R.; MacKnight, C.; Sadovnick, A.D. Diagnosis and treatment of dementia: 1. Risk assessment and primary prevention of Alzheimer disease. *Can. Med. Assoc. J.* **2008**, *178*, 548–556. [[CrossRef](#)]
90. Hansson, O.; Lehmann, S.; Otto, M.; Zetterberg, H.; Lewczuk, P. Advantages and disadvantages of the use of the CSF Amyloid  $\beta$  (A $\beta$ ) 42/40 ratio in the diagnosis of Alzheimer's Disease. *Alzheimer's Res. Ther.* **2019**, *11*, 1–15. [[CrossRef](#)]
91. Klunk, W.E.; Engler, H.; Nordberg, A.; Wang, Y.; Blomqvist, G.; Holt, D.P.; Bergström, M.; Savitcheva, I.; Huang, G.F.; Estrada, S.; et al. Imaging Brain Amyloid in Alzheimer's Disease with Pittsburgh Compound-B. *Ann. Neurol.* **2004**, *55*, 306–319. [[CrossRef](#)] [[PubMed](#)]
92. Rabinovici, G.D.; Furst, A.J.; O'Neil, J.P.; Racine, C.A.; Mormino, E.C.; Baker, S.L.; Chetty, S.; Patel, P.; Pagliaro, T.A.; Klunk, W.E.; et al. 11C-PIB PET imaging in Alzheimer disease and frontotemporal lobar degeneration. *Neurology* **2007**, *68*, 1205–1212. [[CrossRef](#)] [[PubMed](#)]
93. Engler, H.; Santillo, A.F.; Wang, S.X.; Lindau, M.; Savitcheva, I.; Nordberg, A.; Lannfelt, L.; Långström, B.; Kilander, L. In vivo amyloid imaging with PET in frontotemporal dementia. *Eur. J. Nucl. Med. Mol. Imaging* **2008**, *35*, 100–106. [[CrossRef](#)]
94. Lowe, V.J.; Kemp, B.J.; Jack, C.R.; Senjem, M.; Weigand, S.; Shiung, M.; Smith, G.; Knopman, D.; Boeve, B.; Mullan, B.; et al. Comparison of 18F-FDG and PiB PET in cognitive impairment. *J. Nucl. Med.* **2009**, *50*, 878–886. [[CrossRef](#)] [[PubMed](#)]
95. Devanand, D.P.; Mikhno, A.; Pelton, G.H.; Cuasay, K.; Pradhaban, G.; Dileep Kumar, J.S.; Upton, N.; Lai, R.; Gunn, R.N.; Libri, V.; et al. Pittsburgh compound B (11C-PIB) and fluorodeoxyglucose (18 F-FDG) PET in patients with Alzheimer disease, mild cognitive impairment, and healthy controls. *J. Geriatr. Psychiatry Neurol.* **2010**, *23*, 185–198. [[CrossRef](#)]
96. Leuzy, A.; Chiotis, K.; Hasselbalch, S.G.; Rinne, J.O.; De Mendonça, A.; Otto, M.; Lleó, A.; Castelo-Branco, M.; Santana, I.; Johansson, J.; et al. Pittsburgh compound B imaging and cerebrospinal fluid amyloid- $\beta$  in a multicentre European memory clinic study. *Brain* **2016**, *139*, 2540–2553. [[CrossRef](#)] [[PubMed](#)]
97. Sojkova, J.; Driscoll, I.; Iacono, D.; Zhou, Y.; Codispoti, K.-E.; Kraut, M.A.; Ferrucci, L.; Pletnikova, O.; Mathis, C.A.; Klunk, W.E.; et al. In Vivo Fibrillar  $\beta$ -Amyloid Detected Using [11C]PiB Positron Emission Tomography and Neuropathologic Assessment in Older Adults. *Arch. Neurol.* **2011**, *68*, 232–240. [[CrossRef](#)]
98. Clark, C.M.; Pontecorvo, M.J.; Beach, T.G.; Bedell, B.J.; Coleman, R.E.; Doraiswamy, P.M.; Fleisher, A.S.; Reiman, E.M.; Sabbagh, M.N.; Sadowsky, C.H.; et al. Cerebral PET with florbetapir compared with neuropathology at autopsy for detection of neuritic amyloid- $\beta$  plaques: A prospective cohort study. *Lancet Neurol.* **2012**, *11*, 669–678. [[CrossRef](#)]
99. Matveev, S.V.; Spielmann, H.P.; Metts, B.M.; Chen, J.; Onono, F.; Zhu, H.; Scheff, S.W.; Walker, L.C.; LeVine 3rd, H. A distinct subfraction of A $\beta$  is responsible for the high-affinity Pittsburgh compound B-binding site in Alzheimer's disease brain. *J. Neurochem.* **2014**, *131*, 356–368. [[CrossRef](#)] [[PubMed](#)]
100. Yamin, G.; Teplow, D.B. Pittsburgh Compound-B (PiB) binds amyloid  $\beta$ -protein protofibrils. *J. Neurochem.* **2017**, *140*, 210–215. [[CrossRef](#)]
101. Svedberg, M.M.; Hall, H.; Hellström-Lindahl, E.; Estrada, S.; Guan, Z.; Nordberg, A.; Långström, B. [(11)C]PiB-amyloid binding and levels of Abeta40 and Abeta42 in postmortem brain tissue from Alzheimer patients. *Neurochem. Int.* **2009**, *54*, 347–357. [[CrossRef](#)]
102. Ono, K.; Tsuji, M. Protofibrils of amyloid- $\beta$  are important targets of a disease-modifying approach for alzheimer's disease. *Int. J. Mol. Sci.* **2020**, *21*, 952. [[CrossRef](#)]
103. Landau, S.M.; Breault, C.; Joshi, A.D.; Pontecorvo, M.; Mathis, C.A.; Jagust, W.J.; Mintun, M.A. Amyloid- $\beta$  imaging with Pittsburgh compound B and florbetapir: Comparing radiotracers and quantification methods. *J. Nucl. Med.* **2013**, *54*, 70–77. [[CrossRef](#)]
104. Cohen, A.D.; Rabinovici, G.D.; Mathis, C.A.; Jagust, W.J.; Klunk, W.E.; Ikonovic, M.D. Using Pittsburgh Compound B for In Vivo PET Imaging of Fibrillar Amyloid-Beta. *Adv. Pharmacol.* **2012**, *64*, 27–81. [[CrossRef](#)]

105. Tomiyama, T.; Nagata, T.; Shimada, H.; Teraoka, R.; Fukushima, A.; Kanemitsu, H.; Takuma, H.; Kuwano, R.; Imagawa, M.; Ataka, S.; et al. A new amyloid  $\beta$  variant favoring oligomerization in Alzheimer's-type dementia. *Ann. Neurol.* **2008**, *63*, 377–387. [[CrossRef](#)] [[PubMed](#)]
106. Shimada, H.; Ataka, S.; Tomiyama, T.; Takechi, H.; Mori, H.; Miki, T. Clinical Course of Patients with Familial Early-Onset Alzheimer's Disease Potentially Lacking Senile Plaques Bearing the E693 $\Delta$  Mutation in Amyloid Precursor Protein. *Dement. Geriatr. Cogn. Disord.* **2011**, *32*, 45–54. [[CrossRef](#)] [[PubMed](#)]
107. Rowe, C.C.; Ackerman, U.; Browne, W.; Mulligan, R.; Pike, K.L.; O'Keefe, G.; Tochon-Danguy, H.; Chan, G.; Berlangieri, S.U.; Jones, G.; et al. Imaging of amyloid  $\beta$  in Alzheimer's disease with 18F-BAY94-9172, a novel PET tracer: Proof of mechanism. *Lancet Neurol.* **2008**, *7*, 129–135. [[CrossRef](#)]
108. Wolk, D.A.; Zhang, Z.; Boudhar, S.; Clark, C.M.; Pontecorvo, M.J.; Arnold, S.E. Amyloid imaging in Alzheimer's disease: Comparison of florbetapir and Pittsburgh compound-B positron emission tomography. *J. Neurol. Neurosurg. Psychiatry* **2012**, *83*, 923–926. [[CrossRef](#)] [[PubMed](#)]
109. Morris, E.; Chalkidou, A.; Hammers, A.; Peacock, J.; Summers, J.; Keevil, S. Diagnostic accuracy of 18F amyloid PET tracers for the diagnosis of Alzheimer's disease: A systematic review and meta-analysis. *Eur. J. Nucl. Med. Mol. Imaging* **2016**, *43*, 374–385. [[CrossRef](#)] [[PubMed](#)]
110. Wong, D.F.; Rosenberg, P.B.; Zhou, Y.; Kumar, A.; Raymont, V.; Ravert, H.T.; Dannals, R.F.; Nandi, A.; Brasic, J.R.; Ye, W.; et al. In vivo imaging of amyloid deposition in Alzheimer disease using the radioligand 18F-AV-45 (florbetapir [corrected] F 18). *J. Nucl. Med.* **2010**, *51*, 913–920. [[CrossRef](#)] [[PubMed](#)]
111. Bao, W.; Jia, H.; Finnema, S.; Cai, Z.; Carson, R.E.; Huang, Y.H. PET Imaging for Early Detection of Alzheimer's Disease: From Pathologic to Physiologic Biomarkers. *PET Clin.* **2017**, *12*, 329–350. [[CrossRef](#)] [[PubMed](#)]
112. Rowe, C.C.; Ellis, K.A.; Rimajova, M.; Bourgeat, P.; Pike, K.E.; Jones, G.; Frapp, J.; Tochon-Danguy, H.; Morandau, L.; O'Keefe, G.; et al. Amyloid imaging results from the Australian Imaging, Biomarkers and Lifestyle (AIBL) study of aging. *Neurobiol. Aging* **2010**, *31*, 1275–1283. [[CrossRef](#)] [[PubMed](#)]
113. Rowe, C.C.; Villemagne, V.L. Brain amyloid imaging. *J. Nucl. Med. Technol.* **2013**, *41*, 11–18. [[CrossRef](#)] [[PubMed](#)]
114. Gordon, B.A.; Blazey, T.M.; Su, Y.; Hari-Raj, A.; Dincer, A.; Flores, S.; Christensen, J.; McDade, E.; Wang, G.; Xiong, C.; et al. Spatial patterns of neuroimaging biomarker change in individuals from families with autosomal dominant Alzheimer's disease: A longitudinal study. *Lancet Neurol.* **2018**, *17*, 241–250. [[CrossRef](#)]
115. Whitwell, J.L.; Tosakulwong, N.; Weigand, S.D.; Graff-Radford, J.; Duffy, J.R.; Clark, H.M.; Machulda, M.M.; Botha, H.; Utianski, R.L.; Schwarz, C.G.; et al. Longitudinal Amyloid- $\beta$  PET in Atypical Alzheimer's Disease and Frontotemporal Lobar Degeneration. *J. Alzheimers. Dis.* **2020**, *74*, 377–389. [[CrossRef](#)]
116. Wolk, D.A. Amyloid imaging in atypical presentations of Alzheimer's disease. *Curr. Neurol. Neurosci. Rep.* **2013**, *13*, 1–10. [[CrossRef](#)]
117. Villemagne, V.L.; Fodero-Tavoletti, M.T.; Masters, C.L.; Rowe, C.C. Tau imaging: Early progress and future directions. *Lancet Neurol.* **2015**, *14*, 114–124. [[CrossRef](#)]
118. Götz, J.; Ittner, L.M. Animal models of Alzheimer's disease and frontotemporal dementia. *Nat. Rev. Neurosci.* **2008**, *9*, 532–544. [[CrossRef](#)]
119. McLean, C.A.; Cherny, R.A.; Fraser, F.W.; Fuller, S.J.; Smith, M.J.; Beyreuther, K.; Bush, A.I.; Masters, C.L. Soluble pool of A $\beta$  amyloid as a determinant of severity of neurodegeneration in Alzheimer's disease. *Ann. Neurol.* **1999**, *46*, 860–866. [[CrossRef](#)]
120. Goedert, M.; Crowther, R.A.; Garner, C.C. Molecular characterization of microtubule-associated proteins tau and map2. *Trends Neurosci.* **1991**, *14*, 193–199. [[CrossRef](#)]
121. Martin, L.; Latypova, X.; Terro, F. Post-translational modifications of tau protein: Implications for Alzheimer's disease. *Neurochem. Int.* **2011**, *58*, 458–471. [[CrossRef](#)]
122. Noble, W.; Hanger, D.P.; Miller, C.C.J.; Lovestone, S. The importance of tau phosphorylation for neurodegenerative diseases. *Front. Neurol.* **2013**, *4* JUL, 1–11. [[CrossRef](#)]
123. Wu, X.L.; Piña-Crespo, J.; Zhang, Y.W.; Chen, X.C.; Xu, H.X. Tau-mediated neurodegeneration and potential implications in diagnosis and treatment of Alzheimer's disease. *Chin. Med. J.* **2017**, *130*, 2978–2990. [[CrossRef](#)]
124. Saint-Aubert, L.; Lemoine, L.; Chiotis, K.; Leuzy, A.; Rodriguez-Vieitez, E.; Nordberg, A. Tau PET imaging: Present and future directions. *Mol. Neurodegener.* **2017**, *12*, 1–21. [[CrossRef](#)]
125. Ossenkoppele, R.; Cohn-Sheehy, B.I.; La Joie, R.; Vogel, J.W.; Möller, C.; Lehmann, M.; Van Berckel, B.N.M.; Seeley, W.W.; Pijnenburg, Y.A.; Gorno-Tempini, M.L.; et al. Atrophy patterns in early clinical stages across distinct phenotypes of Alzheimer's disease. *Hum. Brain Mapp.* **2015**, *36*, 4421–4437. [[CrossRef](#)] [[PubMed](#)]
126. Sintini, I.; Martin, P.R.; Graff-Radford, J.; Senjem, M.L.; Schwarz, C.G.; Machulda, M.M.; Spychalla, A.J.; Drubach, D.A.; Knopman, D.S.; Petersen, R.C.; et al. Longitudinal tau-PET uptake and atrophy in atypical Alzheimer's disease. *NeuroImage Clin.* **2019**, *23*, 1–12. [[CrossRef](#)]
127. Villemagne, V.L.; Okamura, N. In vivo tau imaging: Obstacles and progress. *Alzheimer's Dement.* **2014**, *10*, 254–264. [[CrossRef](#)]
128. Fitzpatrick, A.W.P.; Falcon, B.; He, S.; Murzin, A.G.; Murshudov, G.; Garringer, H.J.; Crowther, R.A.; Ghetti, B.; Goedert, M.; Scheres, S.H.W. Cryo-EM structures of tau filaments from Alzheimer's disease. *Nature* **2017**, *547*, 185–190. [[CrossRef](#)] [[PubMed](#)]

129. Murugan, N.A.; Nordberg, A.; Ågren, H. Different Positron Emission Tomography Tau Tracers Bind to Multiple Binding Sites on the Tau Fibril: Insight from Computational Modeling. *ACS Chem. Neurosci.* **2018**, *9*, 1757–1767. [[CrossRef](#)] [[PubMed](#)]
130. Harada, R.; Okamura, N.; Furumoto, S.; Tago, T.; Yanai, K.; Arai, H.; Kudo, Y. Characteristics of tau and its ligands in PET imaging. *Biomolecules* **2016**, *6*, 2–15. [[CrossRef](#)] [[PubMed](#)]
131. Shoghi-Jadid, K.; Small, G.W.; Agdeppa, E.D.; Kepe, V.; Ercoli, L.M.; Siddarth, P.; Read, S.; Satyamurthy, N.; Petric, A.; Huang, S.C.; et al. Localization of neurofibrillary tangles and beta-amyloid plaques in the brains of living patients with Alzheimer disease. *Am. J. Geriatr. Psychiatry* **2002**, *10*, 24–35. [[CrossRef](#)] [[PubMed](#)]
132. Maruyama, M.; Shimada, H.; Suhara, T.; Shinotoh, H.; Ji, B.; Maeda, J.; Zhang, M.R.; Trojanowski, J.Q.; Lee, V.M.Y.; Ono, M.; et al. Imaging of tau pathology in a tauopathy mouse model and in Alzheimer patients compared to normal controls. *Neuron* **2013**, *79*, 1094–1108. [[CrossRef](#)] [[PubMed](#)]
133. Okamura, N.; Suemoto, T.; Furumoto, S.; Suzuki, M.; Shimadzu, H.; Akatsu, H.; Yamamoto, T.; Fujiwara, H.; Nemoto, M.; Maruyama, M.; et al. Quinoline and benzimidazole derivatives: Candidate probes for in vivo imaging of tau pathology in Alzheimer's disease. *J. Neurosci.* **2005**, *25*, 10857–10862. [[CrossRef](#)]
134. Okamura, N.; Furumoto, S.; Harada, R.; Tago, T.; Yoshikawa, T.; Fodero-Tavoletti, M.; Mulligan, R.S.; Villemagne, V.L.; Akatsu, H.; Yamamoto, T.; et al. Novel 18F-labeled arylquinoline derivatives for noninvasive imaging of Tau pathology in Alzheimer disease. *J. Nucl. Med.* **2013**, *54*, 1420–1427. [[CrossRef](#)]
135. Harada, R.; Okamura, N.; Furumoto, S.; Furukawa, K.; Ishiki, A.; Tomita, N.; Hiraoka, K.; Watanuki, S.; Shidahara, M.; Miyake, M.; et al. [18F]THK-5117 PET for assessing neurofibrillary pathology in Alzheimer's disease. *Eur. J. Nucl. Med. Mol. Imaging* **2015**, *42*, 1052–1061. [[CrossRef](#)] [[PubMed](#)]
136. Okamura, N.; Furumoto, S.; Fodero-Tavoletti, M.T.; Mulligan, R.S.; Harada, R.; Yates, P.; Pejaska, S.; Kudo, Y.; Masters, C.L.; Yanai, K.; et al. Non-invasive assessment of Alzheimer's disease neurofibrillary pathology using 18F-THK5105 PET. *Brain* **2014**, *137*, 1762–1771. [[CrossRef](#)]
137. Harada, R.; Okamura, N.; Furumoto, S.; Furukawa, K.; Ishiki, A.; Tomita, N.; Tago, T.; Hiraoka, K.; Watanuki, S.; Shidahara, M.; et al. 18F-THK5351: A novel PET radiotracer for imaging neurofibrillary pathology in Alzheimer disease. *J. Nucl. Med.* **2016**, *57*, 208–214. [[CrossRef](#)] [[PubMed](#)]
138. Betthausen, T.J.; Lao, P.J.; Murali, D.; Barnhart, T.E.; Furumoto, S.; Okamura, N.; Stone, C.K.; Johnson, S.C.; Christian, B.T. In vivo comparison of tau radioligands 18F-THK-5351 and 18F-THK-5317. *J. Nucl. Med.* **2017**, *58*, 996–1002. [[CrossRef](#)]
139. Chien, D.T.; Bahri, S.; Szardenings, A.K.; Walsh, J.C.; Mu, F.; Su, M.Y.; Shankle, W.R.; Elizarov, A.; Kolb, H.C. Early Clinical PET Imaging Results with the Novel PHF-Tau Radioligand [F-18]-T807. *J. Alzheimer's Dis.* **2013**, *34*, 457–468. [[CrossRef](#)]
140. Das, S.R.; Xie, L.; Wisse, L.E.M.; Ittyerah, R.; Tustison, N.J.; Dickerson, B.C.; Yushkevich, P.A.; Wolk, D.A. Longitudinal and cross-sectional structural magnetic resonance imaging correlates of AV-1451 uptake. *Neurobiol. Aging* **2018**, *66*, 49–58. [[CrossRef](#)]
141. Chien, D.T.; Szardenings, A.K.; Bahri, S.; Walsh, J.C.; Mu, F.; Xia, C.; Shankle, W.R.; Lerner, A.J.; Su, M.Y.; Elizarov, A.; et al. Early clinical PET imaging results with the novel PHF-tau radioligand [F18]-T808. *J. Alzheimer's Dis.* **2014**, *38*, 171–184. [[CrossRef](#)]
142. Marquié, M.; Normandin, M.D.; Meltzer, A.C.; Siao Tick Chong, M.; Andrea, N.V.; Antón-Fernández, A.; Klunk, W.E.; Mathis, C.A.; Ikonovic, M.D.; Debnath, M.; et al. Pathological correlations of [F-18]-AV-1451 imaging in non-Alzheimer tauopathies. *Ann. Neurol.* **2017**, *81*, 117–128. [[CrossRef](#)]
143. Kimura, Y.; Ichise, M.; Ito, H.; Shimada, H.; Ikoma, Y.; Seki, C.; Takano, H.; Kitamura, S.; Shinotoh, H.; Kawamura, K.; et al. PET quantification of tau pathology in human brain with 11C-PBB3. *J. Nucl. Med.* **2015**, *56*, 1359–1365. [[CrossRef](#)]
144. Hashimoto, H.; Kawamura, K.; Igarashi, N.; Takei, M.; Fujishiro, T.; Aihara, Y.; Shiomi, S.; Muto, M.; Ito, T.; Furutsuka, K.; et al. Radiosynthesis, photoisomerization, biodistribution, and metabolite analysis of 11C-PBB3 as a clinically useful PET probe for imaging of tau pathology. *J. Nucl. Med.* **2014**, *55*, 1532–1538. [[CrossRef](#)] [[PubMed](#)]
145. Goedert, M. Alzheimer's and Parkinson's diseases: The prion concept in relation to assembled A $\beta$ , tau, and  $\alpha$ -synuclein. *Science* (80-. ). **2015**, *349*, 1255–1255. [[CrossRef](#)]
146. Frisoni, G.B.; Boccardi, M.; Barkhof, F.; Blennow, K.; Cappa, S.; Chiotis, K.; Démonet, J.F.; Garibotto, V.; Giannakopoulos, P.; Gietl, A.; et al. Strategic roadmap for an early diagnosis of Alzheimer's disease based on biomarkers. *Lancet Neurol.* **2017**, *16*, 661–676. [[CrossRef](#)]
147. Fox, N.C.; Scahill, R.I.; Crum, W.R.; Rossor, M.N. Correlation between rates of brain atrophy and cognitive decline in AD. *Neurology* **1999**, *52*, 1687–1689. [[CrossRef](#)] [[PubMed](#)]
148. Sluimer, J.D.; van der Flier, W.M.; Karas, G.B.; Fox, N.C.; Scheltens, P.; Barkhof, F.; Vrenken, H. Whole-Brain Atrophy Rate and Cognitive Decline: Longitudinal MR Study of Memory Clinic Patients 1 Purpose: Methods: Results: Conclusion. *Radiology* **2008**, *248*, 590–598. [[CrossRef](#)] [[PubMed](#)]
149. Schott, J.M.; Crutch, S.J.; Frost, C.; Warrington, E.K.; Rossor, M.N.; Fox, N.C. Neuropsychological correlates of whole brain atrophy in Alzheimer's disease. *Neuropsychologia* **2008**, *46*, 1732–1737. [[CrossRef](#)]
150. Cardenas, V.A.; Chao, L.L.; Studholme, C.; Yaffe, K.; Miller, B.L.; Madison, C.; Buckley, S.T.; Mungas, D.; Schuff, N.; Weiner, M.W. Brain atrophy associated with baseline and longitudinal measures of cognition. *Neurobiol. Aging* **2011**, *32*, 572–580. [[CrossRef](#)] [[PubMed](#)]
151. Thompson, P.M.; Hayashi, K.M.; De Zubicaray, G.I.; Janke, A.L.; Rose, S.E.; Semple, J.; Hong, M.S.; Herman, D.H.; Gravano, D.; Doddrell, D.M.; et al. Mapping hippocampal and ventricular change in Alzheimer disease. *Neuroimage* **2004**, *22*, 1754–1766. [[CrossRef](#)] [[PubMed](#)]

152. Jack, C.R.; Shiung, M.M.; Gunter, J.L.; O'Brien, P.C.; Weigand, S.D.; Knopman, D.S.; Boeve, B.F.; Ivnik, R.J.; Smith, G.E.; Cha, R.H.; et al. Comparison of different MRI brain atrophy rate measures with clinical disease progression in AD. *Neurology* **2004**, *62*, 591–600. [[CrossRef](#)]
153. Creavin, S.T.; Wisniewski, S.; Noel-Storr, A.H.; Trevelyan, C.M.; Hampton, T.; Rayment, D.; Thom, V.M.; Nash, K.J.E.; Elhamoui, H.; Milligan, R.; et al. Mini-Mental State Examination (MMSE) for the detection of dementia in clinically unevaluated people aged 65 and over in community and primary care populations. *Cochrane Database Syst. Rev.* **2016**. [[CrossRef](#)]
154. Ossenkoppele, R.; Pijnenburg, Y.A.L.; Perry, D.C.; Cohn-Sheehy, B.I.; Scheltens, N.M.E.; Vogel, J.W.; Kramer, J.H.; Van Der Vlies, A.E.; Joie, R.L.; Rosen, H.J.; et al. The behavioural/dysexecutive variant of Alzheimer's disease: Clinical, neuroimaging and pathological features. *Brain* **2015**, *138*, 2732–2749. [[CrossRef](#)]
155. Drzezga, A.; Lautenschlager, N.; Siebner, H.; Riemenschneider, M.; Willoch, F.; Minoshima, S.; Schwaiger, M.; Kurz, A. Cerebral metabolic changes accompanying conversion of mild cognitive impairment into alzheimer's disease: A PET follow-up study. *Eur. J. Nucl. Med. Mol. Imaging* **2003**, *30*, 1104–1113. [[CrossRef](#)] [[PubMed](#)]
156. Fouquet, M.; Desgranges, B.; Landeau, B.; Duchesnay, E.; Mzenge, F.; De La Sayette, V.; Viader, F.; Baron, J.C.; Eustache, F.; Chtelat, G. Longitudinal brain metabolic changes from amnesic mild cognitive impairment to Alzheimers disease. *Brain* **2009**, *132*, 2058–2067. [[CrossRef](#)] [[PubMed](#)]
157. Bradley, K.M.; O'Sullivan, V.T.; Soper, N.D.W.; Nagy, Z.; King, E.M.-F.; Smith, A.D.; Shepstone, B.J. Cerebral perfusion SPET correlated with Braak pathological stage in Alzheimer's disease. *Brain* **2002**, *125*, 1772–1781. [[CrossRef](#)]
158. Petersen, R.C.; Aisen, P.S.; Beckett, L.A.; Donohue, M.C.; Gamst, A.C.; Harvey, D.J.; Jack, C.R.; Jagust, W.J.; Shaw, L.M.; Toga, A.W.; et al. Alzheimer's Disease Neuroimaging Initiative (ADNI): Clinical characterization. *Neurology* **2010**, *74*, 201–209. [[CrossRef](#)]
159. Aisen, P.S.; Petersen, R.C.; Donohue, M.C.; Gamst, A.; Raman, R.; Thomas, R.G.; Walter, S.; Trojanowski, J.Q.; Shaw, L.M.; Beckett, L.A.; et al. Clinical core of the Alzheimer's disease neuroimaging initiative: Progress and plans. *Alzheimers Dement.* **2010**, *6*, 239–246. [[CrossRef](#)]
160. Kim, S.H.; Seo, S.W.; Yoon, D.S.; Chin, J.; Lee, B.H.; Cheong, H.-K.; Han, S.-H.; Na, D.L. Comparison of neuropsychological and FDG-PET findings between early- versus late-onset mild cognitive impairment: A five-year longitudinal study. *Dement. Geriatr. Cogn. Disord.* **2010**, *29*, 213–223. [[CrossRef](#)]
161. Anchisi, D.; Borroni, B.; Franceschi, M.; Kerrouche, N.; Kalbe, E.; Beuthien-Beumann, B.; Cappa, S.; Lenz, O.; Ludecke, S.; Marcone, A.; et al. Heterogeneity of brain glucose metabolism in mild cognitive impairment and clinical progression to Alzheimer disease. *Arch. Neurol.* **2005**, *62*, 1728–1733. [[CrossRef](#)] [[PubMed](#)]
162. Drzezga, A.; Grimmer, T.; Riemenschneider, M.; Lautenschlager, N.; Siebner, H.; Alexopoulos, P.; Minoshima, S.; Schwaiger, M.; Kurz, A. Prediction of individual clinical outcome in MCI by means of genetic assessment and (18)F-FDG PET. *J. Nucl. Med.* **2005**, *46*, 1625–1632.
163. Mosconi, L.; Perani, D.; Sorbi, S.; Herholz, K.; Nacmias, B.; Holthoff, V.; Salmon, E.; Baron, J.-C.; De Cristofaro, M.T.R.; Padovani, A.; et al. MCI conversion to dementia and the APOE genotype: A prediction study with FDG-PET. *Neurology* **2004**, *63*, 2332–2340. [[CrossRef](#)] [[PubMed](#)]
164. Sohn, B.K.; Yi, D.; Seo, E.H.; Choe, Y.M.; Kim, J.W.; Kim, S.G.; Choi, H.J.; Byun, M.S.; Jhoo, J.H.; Woo, J.I.; et al. Comparison of regional gray matter atrophy, white matter alteration, and glucose metabolism as a predictor of the conversion to alzheimer's disease in mild cognitive impairment. *J. Korean Med. Sci.* **2015**, *30*, 779–787. [[CrossRef](#)] [[PubMed](#)]
165. Vanhoutte, M.; Semah, F.; Leclerc, X.; Sillaire, A.R.; Jaillard, A.; Kuchcinski, G.; Delbeuck, X.; Fahmi, R.; Pasquier, F.; Lopes, R. Three-year changes of cortical 18F-FDG in amnesic vs. non-amnesic sporadic early-onset Alzheimer's disease. *Eur. J. Nucl. Med. Mol. Imaging* **2020**, *47*, 304–318. [[CrossRef](#)]
166. Ishibashi, K.; Onishi, A.; Wagatsuma, K.; Fujiwara, Y.; Ishii, K. Longitudinal 18F-FDG Images in Patients with Alzheimer Disease over More Than 9 Years from a Preclinical Stage. *Clin. Nucl. Med.* **2020**, *45*, E185–E189. [[CrossRef](#)] [[PubMed](#)]
167. Vanhoutte, M.; Semah, F.; Rollin Sillaire, A.; Jaillard, A.; Petyt, G.; Kuchcinski, G.; Maureille, A.; Delbeuck, X.; Fahmi, R.; Pasquier, F.; et al. 18F-FDG PET hypometabolism patterns reflect clinical heterogeneity in sporadic forms of early-onset Alzheimer's disease. *Neurobiol. Aging* **2017**, *59*, 184–196. [[CrossRef](#)]
168. Cerami, C.; Della Rosa, P.A.; Magnani, G.; Santangelo, R.; Marcone, A.; Cappa, S.F.; Perani, D. Brain metabolic maps in Mild Cognitive Impairment predict heterogeneity of progression to dementia. *NeuroImage Clin.* **2015**, *7*, 187–194. [[CrossRef](#)] [[PubMed](#)]
169. Kas, A.; Migliaccio, R.; Tavitian, B. A future for PET imaging in Alzheimer's disease. *Eur. J. Nucl. Med. Mol. Imaging* **2020**, *47*, 231–234. [[CrossRef](#)]
170. Caminiti, S.P.; Ballarini, T.; Sala, A.; Cerami, C.; Presotto, L.; Santangelo, R.; Fallanca, F.; Vanoli, E.G.; Gianolli, L.; Iannaccone, S.; et al. FDG-PET and CSF biomarker accuracy in prediction of conversion to different dementias in a large multicentre MCI cohort. *NeuroImage Clin.* **2018**, *18*, 167–177. [[CrossRef](#)] [[PubMed](#)]
171. Byrnes, K.R.; Wilson, C.M.; Brabazon, F.; von Leden, R.; Jurgens, J.S.; Oakes, T.R.; Selwyn, R.G. FDG-PET imaging in mild traumatic brain injury: A critical review. *Front. Neuroenergetics* **2014**, *5*, 13. [[CrossRef](#)]
172. Longstreth, W.T.J.; Bernick, C.; Manolio, T.A.; Bryan, N.; Jungreis, C.A.; Price, T.R. Lacunar infarcts defined by magnetic resonance imaging of 3660 elderly people: The Cardiovascular Health Study. *Arch. Neurol.* **1998**, *55*, 1217–1225. [[CrossRef](#)]

173. Shokouhi, S.; Campbell, D.; Brill, A.B.; Gwirtsman, H.E. Longitudinal Positron Emission Tomography in Preventive Alzheimer's Disease Drug Trials, Critical Barriers from Imaging Science Perspective. *Brain Pathol.* **2016**, *26*, 664–671. [[CrossRef](#)] [[PubMed](#)]
174. Ou, Y.N.; Xu, W.; Li, J.Q.; Guo, Y.; Cui, M.; Chen, K.L.; Huang, Y.Y.; Dong, Q.; Tan, L.; Yu, J.T. FDG-PET as an independent biomarker for Alzheimer's biological diagnosis: A longitudinal study. *Alzheimer's Res. Ther.* **2019**, *11*, 1–11. [[CrossRef](#)] [[PubMed](#)]
175. Villemagne, V.L.; Pike, K.E.; Chételat, G.; Ellis, K.A.; Mulligan, R.S.; Bourgeat, P.; Ackermann, U.; Jones, G.; Szoëke, C.; Salvado, O.; et al. Longitudinal assessment of A $\beta$  and cognition in aging and Alzheimer disease. *Ann. Neurol.* **2011**, *69*, 181–192. [[CrossRef](#)] [[PubMed](#)]
176. Jagust, W. Imaging the evolution and pathophysiology of Alzheimer disease. *Nat. Rev. Neurosci.* **2018**, *19*, 687–700. [[CrossRef](#)]
177. Koivunen, J.; Scheinin, N.; Virta, J.R.; Aalto, S.; Vahlberg, T.; Helin, S.; Parkkola, R.; Viitanen, M.; Rinne, J.O. Amyloid PET imaging in patients with mild cognitive impairment. *Neurology* **2011**, 1085–1090. [[CrossRef](#)]
178. Ossenkoppele, R.; Tolboom, N.; Foster-Dingley, J.C.; Adriaanse, S.F.; Boellaard, R.; Yaqub, M.; Windhorst, A.D.; Barkhof, F.; Lammertsma, A.A.; Scheltens, P.; et al. Longitudinal imaging of Alzheimer pathology using [ $^{11}\text{C}$ ]PIB, [ $^{18}\text{F}$ ]FDDNP and [ $^{18}\text{F}$ ]FDG PET. *Eur. J. Nucl. Med. Mol. Imaging* **2012**, *39*, 990–1000. [[CrossRef](#)]
179. Villemagne, V.L.; Burnham, S.; Bourgeat, P.; Brown, B.; Ellis, K.A.; Salvado, O.; Szoëke, C.; Macaulay, S.L.; Martins, R.; Maruff, P.; et al. Amyloid  $\beta$  deposition, neurodegeneration, and cognitive decline in sporadic Alzheimer's disease: A prospective cohort study. *Lancet Neurol.* **2013**, *12*, 357–367. [[CrossRef](#)]
180. Jack, C.R.; Wiste, H.J.; Lesnick, T.G.; Weigand, S.D.; Knopman, D.S.; Vemuri, P.; Pankratz, V.S.; Senjem, M.L.; Gunter, J.L.; Mielke, M.M.; et al. Brain  $\beta$ -amyloid load approaches a plateau. *Neurology* **2013**, *80*, 890–896. [[CrossRef](#)]
181. Chen, K.; Roontiva, A.; Thiyyagura, P.; Lee, W.; Liu, X.; Ayutyanont, N.; Protas, H.; Luo, J.L.; Bauer, R.; Reschke, C.; et al. Improved power for characterizing longitudinal amyloid- $\beta$ PET changes and evaluating amyloid-modifying treatments with a cerebral white matter reference region. *J. Nucl. Med.* **2015**, *56*, 560–566. [[CrossRef](#)]
182. Shokouhi, S.; McKay, J.W.; Baker, S.L.; Kang, H.; Brill, A.B.; Gwirtsman, H.E.; Riddle, W.R.; Claassen, D.O.; Rogers, B.P. Reference tissue normalization in longitudinal  $^{18}\text{F}$ -florbetapir positron emission tomography of late mild cognitive impairment. *Alzheimer's Res. Ther.* **2016**, *8*, 2. [[CrossRef](#)] [[PubMed](#)]
183. Landau, S.M.; Fero, A.; Baker, S.L.; Koeppe, R.; Mintun, M.; Chen, K.; Reiman, E.M.; Jagust, W.J. Measurement of longitudinal  $\beta$ -amyloid change with  $^{18}\text{F}$ -florbetapir PET and standardized uptake value ratios. *J. Nucl. Med.* **2015**, *56*, 567–574. [[CrossRef](#)] [[PubMed](#)]
184. Villemagne, V.L.; Doré, V.; Bourgeat, P.; Burnham, S.C.; Laws, S.; Salvado, O.; Masters, C.L.; Rowe, C.C. A $\beta$ -amyloid and Tau Imaging in Dementia. *Semin. Nucl. Med.* **2017**, *47*, 75–88. [[CrossRef](#)]
185. Bischof, G.N.; Endepols, H.; van Eimeren, T.; Drzezga, A. Tau-imaging in neurodegeneration. *Methods* **2017**, *130*, 114–123. [[CrossRef](#)]
186. Ishiki, A.; Okamura, N.; Furukawa, K.; Furumoto, S.; Harada, R.; Tomita, N.; Hiraoka, K.; Watanuki, S.; Ishikawa, Y.; Tago, T.; et al. Longitudinal assessment of Tau pathology in patients with Alzheimer's disease using [ $^{18}\text{F}$ ] THK-5117 positron emission tomography. *PLoS ONE* **2015**, *10*, e0140311. [[CrossRef](#)]
187. Jack, C.R.; Wiste, H.J.; Schwarz, C.G.; Lowe, V.J.; Senjem, M.L.; Vemuri, P.; Weigand, S.D.; Therneau, T.M.; Knopman, D.S.; Gunter, J.L.; et al. Longitudinal tau PET in ageing and Alzheimer's disease. *Brain* **2018**, *141*, 1517–1528. [[CrossRef](#)] [[PubMed](#)]
188. Harrison, T.M.; La Joie, R.; Maass, A.; Baker, S.L.; Swinnerton, K.; Fenton, L.; Mellinger, T.J.; Edwards, L.; Pham, J.; Miller, B.L.; et al. Longitudinal tau accumulation and atrophy in aging and Alzheimer disease. *Ann. Neurol.* **2019**, *85*, 229–240. [[CrossRef](#)]
189. Cho, H.; Choi, J.Y.; Lee, H.S.; Lee, J.H.; Ryu, Y.H.; Lee, M.S.; Jack, C.R.; Lyoo, C.H. Progressive tau accumulation in Alzheimer disease: 2-year follow-up study. *J. Nucl. Med.* **2019**, *60*, 1611–1621. [[CrossRef](#)]
190. Vogels, T.; Leuzy, A.; Cicognola, C.; Ashton, N.J.; Smolek, T.; Novak, M.; Blennow, K.; Zetterberg, H.; Hromadka, T.; Zilka, N.; et al. Propagation of Tau Pathology: Integrating Insights From Postmortem and In Vivo Studies. *Biol. Psychiatry* **2020**, *87*, 808–818. [[CrossRef](#)]
191. Krajcovicova, L.; Klobusiakova, P.; Rektorova, I. Gray Matter Changes in Parkinson's and Alzheimer's Disease and Relation to Cognition. *Curr. Neurol. Neurosci. Rep.* **2019**, *19*. [[CrossRef](#)] [[PubMed](#)]
192. Jeon, S.; Kang, J.M.; Seo, S.; Jeong, H.J.; Funck, T.; Lee, S.Y.; Park, K.H.; Lee, Y.B.; Yeon, B.K.; Ido, T.; et al. Topographical heterogeneity of Alzheimer's disease based on MR imaging, tau PET, and amyloid PET. *Front. Aging Neurosci.* **2019**, *10*, 1–10. [[CrossRef](#)] [[PubMed](#)]
193. Ashburner, J.; Friston, K.J. Voxel-based morphometry—The methods. *Neuroimage* **2000**, *11*, 805–821. [[CrossRef](#)]
194. Matsuda, H. MRI morphometry in Alzheimer's disease. *Ageing Res. Rev.* **2016**, *30*, 17–24. [[CrossRef](#)] [[PubMed](#)]
195. Schmitter, D.; Roche, A.; Maréchal, B.; Ribes, D.; Abdulkadir, A.; Bach-Cuadra, M.; Daducci, A.; Granziera, C.; Klöppel, S.; Maeder, P.; et al. An evaluation of volume-based morphometry for prediction of mild cognitive impairment and Alzheimer's disease. *NeuroImage Clin.* **2015**, *7*, 7–17. [[CrossRef](#)]
196. Friese, U.; Meindl, T.; Herpertz, S.C.; Reiser, M.F.; Hampel, H.G.; Teipel, S.J. Diagnostic utility of novel mri-Based biomarkers for Alzheimer's disease: Diffusion tensor imaging and deformation-based morphometry. *J. Alzheimer's Dis.* **2010**, *20*, 477–490. [[CrossRef](#)]

197. Manera, A.L.; Dadar, M.; Collins, D.L.; Ducharme, S. Deformation based morphometry study of longitudinal MRI changes in behavioral variant frontotemporal dementia. *NeuroImage Clin.* **2019**, *24*, 102079. [[CrossRef](#)] [[PubMed](#)]
198. Hua, X.; Leow, A.D.; Parikshak, N.; Lee, S.; Chiang, M.-C.; Toga, A.W.; Jack, C.R., Jr.; Weiner, M.W.; Thompson, P.M.; Initiative, A.D.N. Tensor-based morphometry as a neuroimaging biomarker for Alzheimer's disease: An MRI study of 676 AD, MCI, and normal subjects. *Neuroimage* **2008**, *43*, 458–469. [[CrossRef](#)]
199. Gaonkar, B.; Pohl, K.; Davatzikos, C. Pattern Based Morphometry. In Proceedings of the International Conference on Medical Image Computing and Computer-Assisted Intervention, Toronto, ON, Canada, 18–22 September 2011; pp. 459–466. [[CrossRef](#)]
200. Jiang, J.; Sun, Y.; Zhou, H.; Li, S.; Huang, Z.; Wu, P.; Shi, K.; Zuo, C.; Alzheimer's Disease Neuroimaging Initiative. Study of the Influence of Age in 18 F-FDG PET Images Using a Data-Driven Approach and Its Evaluation in Alzheimer's Disease. *Contrast Media Mol. Imaging* **2018**, *2018*, 3786083. [[CrossRef](#)] [[PubMed](#)]
201. Vogel, J.W.; Mattsson, N.; Iturria-Medina, Y.; Strandberg, O.T.; Schöll, M.; Dansereau, C.; Villeneuve, S.; van der Flier, W.M.; Scheltens, P.; Bellec, P.; et al. Data-driven approaches for tau-PET imaging biomarkers in Alzheimer's disease. *Hum. Brain Mapp.* **2019**, *40*, 638–651. [[CrossRef](#)] [[PubMed](#)]
202. Chandra, A.; Dervenoulas, G.; Politis, M. Magnetic resonance imaging in Alzheimer's disease and mild cognitive impairment. *J. Neurol.* **2019**, *266*, 1293–1302. [[CrossRef](#)] [[PubMed](#)]
203. Teipel, S.J.; Walter, M.; Licitjaroen, Y.; Schönknecht, P.; Gruber, O. Diffusion tensor imaging in Alzheimer's disease and affective disorders. *Eur. Arch. Psychiatry Clin. Neurosci.* **2014**, *264*, 467–483. [[CrossRef](#)] [[PubMed](#)]
204. Brueggen, K.; Dyrba, M.; Barkhof, F.; Hausner, L.; Filippi, M.; Nestor, P.J.; Hauenstein, K.; Klöppel, S.; Grothe, M.J.; Kasper, E.; et al. Basal forebrain and hippocampus as predictors of conversion to Alzheimer's disease in patients with mild cognitive impairment—a multicenter DTI and volumetry study. *J. Alzheimer's Dis.* **2015**, *48*, 197–204. [[CrossRef](#)] [[PubMed](#)]
205. Fjell, A.M.; Amlien, I.K.; Westlye, L.T.; Walhovd, K.B. Mini-mental state examination is sensitive to brain atrophy in Alzheimer's disease. *Dement. Geriatr. Cogn. Disord.* **2009**, *28*, 252–258. [[CrossRef](#)] [[PubMed](#)]
206. Heo, J.-H.; Lee, S.-T.; Chu, K.; Park, H.-J.; Shim, J.-Y.; Kim, M. White matter hyperintensities and cognitive dysfunction in Alzheimer disease. *J. Geriatr. Psychiatry Neurol.* **2009**, *22*, 207–212. [[CrossRef](#)]
207. Hoy, A.R.; Ly, M.; Carlsson, C.M.; Okonkwo, O.C.; Zetterberg, H.; Blennow, K.; Sager, M.A.; Asthana, S.; Johnson, S.C.; Alexander, A.L.; et al. Microstructural white matter alterations in preclinical Alzheimer's disease detected using free water elimination diffusion tensor imaging. *PLoS ONE* **2017**, *12*, e0173982. [[CrossRef](#)] [[PubMed](#)]
208. Sperling, R. The potential of functional MRI as a biomarker in early Alzheimer's disease. *Neurobiol. Aging* **2011**, *32*, 1–11. [[CrossRef](#)]
209. Hojjati, S.H.; Ebrahimzadeh, A.; Babajani-Feremi, A. Identification of the early stage of Alzheimer's disease using structural MRI and resting-state fMRI. *Front. Neurol.* **2019**, *10*, 1–12. [[CrossRef](#)] [[PubMed](#)]
210. Greicius, M.D.; Krasnow, B.; Reiss, A.L.; Menon, V. Functional connectivity in the resting brain: A network analysis of the default mode hypothesis. *Proc. Natl. Acad. Sci.* **2003**, *100*, 253–258. [[CrossRef](#)]
211. Das, S.R.; Pluta, J.; Mancuso, L.; Kliot, D.; Orozco, S.; Dickerson, B.C.; Yushkevich, P.A.; Wolk, D.A. Increased functional connectivity within medial temporal lobe in mild cognitive impairment. *Hippocampus* **2013**, *23*, 1–6. [[CrossRef](#)]
212. Yu, E.; Liao, Z.; Mao, D.; Zhang, Q.; Ji, G.; Li, Y.; Ding, Z. Directed Functional Connectivity of Posterior Cingulate Cortex and Whole Brain in Alzheimer's Disease and Mild Cognitive Impairment. *Curr. Alzheimer Res.* **2017**, *14*, 628–635. [[CrossRef](#)] [[PubMed](#)]
213. Doustar, J.; Torbati, T.; Black, K.L.; Koronyo, Y.; Koronyo-Hamaoui, M. Optical coherence tomography in Alzheimer's disease and other neurodegenerative diseases. *Front. Neurol.* **2017**, *8*, 1–13. [[CrossRef](#)] [[PubMed](#)]
214. Huang, D.; Swanson, E.A.; Lin, C.P.; Schuman, J.S.; Stinson, W.G.; Chang, W.; Hee, M.R.; Flotte, T.; Gregory, K.; Puliafito, C.A.; et al. Optical coherence tomography. *Science* **1991**, *254*, 1178–1181. [[CrossRef](#)] [[PubMed](#)]
215. Günes, A.; Demirci, S.; Tök, L.; Tök, Ö.; Demirci, S. Evaluation of retinal nerve fiber layer thickness in Alzheimer disease using spectral-domain optical coherence tomography. *Turkish J. Med. Sci.* **2015**, *45*, 1094–1097. [[CrossRef](#)]
216. Htike, T.T.; Mishra, S.; Kumar, S.; Padmanabhan, P.; Gulyás, B. Peripheral Biomarkers for Early Detection of Alzheimer's and Parkinson's Diseases. *Mol. Neurobiol.* **2019**, *56*, 2256–2277. [[CrossRef](#)] [[PubMed](#)]
217. Van De Kreeke, J.A.; Nguyen, H.T.; Konijnenberg, E.; Tomassen, J.; Den Braber, A.; Ten Kate, M.; Yaqub, M.; Van Berckel, B.; Lammertsma, A.A.; Boomsma, D.I.; et al. Optical coherence tomography angiography in preclinical Alzheimer's disease. *Br. J. Ophthalmol.* **2019**, 157–161. [[CrossRef](#)]
218. Cabrera DeBuc, D.; Gaca-Wysocka, M.; Grzybowski, A.; Kanclerz, P. Identification of Retinal Biomarkers in Alzheimer's Disease Using Optical Coherence Tomography: Recent Insights, Challenges, and Opportunities. *J. Clin. Med.* **2019**, *8*, 996. [[CrossRef](#)]
219. Mercier, J.; Provins, L.; Valade, A. Discovery and development of SV2A PET tracers: Potential for imaging synaptic density and clinical applications. *Drug Discov. Today Technol.* **2017**, *25*, 45–52. [[CrossRef](#)]
220. Finnema, S.J.; Nabulsi, N.B.; Eid, T.; Detyniecki, K.; Lin, S.F.; Chen, M.K.; Dhaher, R.; Matuskey, D.; Baum, E.; Holden, D.; et al. Imaging synaptic density in the living human brain. *Sci. Transl. Med.* **2016**, *8*, 1–10. [[CrossRef](#)]
221. Kong, Y.; Liu, C.; Zhou, Y.; Qi, J.; Zhang, C.; Sun, B.; Wang, J.; Guan, Y. Progress of RAGE Molecular Imaging in Alzheimer's Disease. *Front. Aging Neurosci.* **2020**, *12*, 1–9. [[CrossRef](#)] [[PubMed](#)]

222. Paudel, Y.N.; Angelopoulou, E.; Piperi, C.; Othman, I.; Aamir, K.; Shaikh, M.F. Impact of HMGB1, RAGE, and TLR4 in Alzheimer's Disease (AD): From Risk Factors to Therapeutic Targeting. *Cells* **2020**, *9*, 383. [[CrossRef](#)]
223. Luzi, F.; Savickas, V.; Taddei, C.; Hader, S.; Singh, N.; Gee, A.D.; Bongarzone, S. Radiolabeling of [11C]FPS-ZM1, a receptor for advanced glycation end products-targeting positron emission tomography radiotracer, using a [11C]CO<sub>2</sub>-to-[11C]CO chemical conversion. *Future Med. Chem.* **2020**, *12*, 511–521. [[CrossRef](#)] [[PubMed](#)]
224. Moon, Y.; Han, S.H.; Moon, W.J. Patterns of Brain Iron Accumulation in Vascular Dementia and Alzheimer's Dementia Using Quantitative Susceptibility Mapping Imaging. *J. Alzheimer's Dis.* **2016**, *51*, 737–745. [[CrossRef](#)] [[PubMed](#)]
225. Zecca, L.; Youdim, M.B.H.; Riederer, P.; Connor, J.R.; Crichton, R.R. Iron, brain ageing and neurodegenerative disorders. *Nat. Rev. Neurosci.* **2004**, *5*, 863–873. [[CrossRef](#)] [[PubMed](#)]
226. Gong, N.J.; Dibb, R.; Bulk, M.; van der Weerd, L.; Liu, C. Imaging beta amyloid aggregation and iron accumulation in Alzheimer's disease using quantitative susceptibility mapping MRI. *Neuroimage* **2019**, *191*, 176–185. [[CrossRef](#)]
227. Kim, H.-G.; Park, S.; Rhee, H.Y.; Lee, K.M.; Ryu, C.W.; Rhee, S.J.; Lee, S.Y.; Wang, Y.; Jahng, G.H. Quantitative susceptibility mapping to evaluate the early stage of Alzheimer's disease. *NeuroImage Clin.* **2017**, *16*, 429–438. [[CrossRef](#)]